International Journal of Plasticity xxx (2013) xxx–xxx

Contents lists available at ScienceDirect

International Journal of Plasticity

journal homepage: www.elsevier.com/locate/ijplas

Dislocation slip stress prediction in shape memory alloys

J. Wang [a], H. Sehitoglu [a,*], H.J. Maier [b]

[a] Department of Mechanical Science and Engineering, University of Illinois at Urbana-Champaign, 1206 W. Green St., Urbana, IL 61801, USA
[b] Institut für Werkstoffkunde, Leibniz Universität Hannover, An der Universität 2, D-30823 Garbsen, Germany

ARTICLE INFO

Article history:
Received 25 March 2013
Received in final revised form 26 August 2013
Available online xxxx

Keywords:
Peierls stress
Extended Peierls–Nabarro model
Shape memory alloy
Dislocation slip
Generalized stacking fault energy

ABSTRACT

We provide an extended Peierls–Nabarro (P–N) formulation with a sinusoidal series representation of generalized stacking fault energy (GSFE) to establish flow stress in a Ni_2FeGa shape memory alloy. The resultant martensite structure in Ni_2FeGa is $L1_0$ tetragonal. The atomistic simulations allowed determination of the GSFE landscapes for the $(1\,1\,1)$ slip plane and $\frac{1}{2}[\bar{1}\,0\,1]$, $\frac{1}{2}[\bar{1}\,1\,0]$, $\frac{1}{6}[\bar{2}\,1\,1]$ and $\frac{1}{6}[1\,1\,\bar{2}]$ slip vectors. The energy barriers in the $(1\,1\,1)$ plane were associated with superlattice intrinsic stacking faults, complex stacking faults and anti-phase boundaries. The smallest energy barrier was determined as 168 mJ/m^2 corresponding to a Peierls stress of 1.1 GPa for the $\frac{1}{6}[1\,1\,\bar{2}](1\,1\,1)$ slip system. Experiments on single crystals of Ni_2FeGa were conducted under tension where the specimen underwent austenite to martensite transformation followed by elasto-plastic martensite deformation. The experimentally determined martensite slip stress (0.75 GPa) was much closer to the P–N stress predictions (1.1 GPa) compared to the theoretical slip stress levels (3.65 GPa). The evidence of dislocation slip in Ni_2FeGa martensite was also identified with transformation electron microscopy observations. We also investigated dislocation slip in several important shape memory alloys and predicted Peierls stresses in Ni_2FeGa, NiTi, Co_2NiGa, Co_2NiAl, CuZn and Ni_2TiHf austenite in excellent agreement with experiments.

© 2013 Elsevier Ltd. All rights reserved.

1. Introduction

1.1. Background

Shape memory alloys with high temperature (Chumlyakov et al., 2008; Hamilton et al., 2006a,b, 2007; Hartl et al., 2010; Oikawa et al., 2003; Omori et al., 2004; Santamarta et al., 2006; Sutou et al., 2004) and magnetic actuation capabilities (Arndt et al., 2006; Brown et al., 2002; Kokorin et al., 1992; Planes et al., 1997; Pons et al., 2005; Ullakko et al., 1996; Zheludev et al., 1996) have generated considerable recent interest. The development of such alloys has traditionally relied on processing of different chemical compositions, making polycrystalline ingots, and then taking the expensive route of making single crystals. Then, the alloys have been tested under temperature or stress cycling, and in the case of ferromagnetic shape memory alloys under applied magnetic fields (Ullakko et al., 1996). Additional tests may be necessary to establish the elastic constants, lattice constants and to determine the twinning stress and the slip stress of the austenite and martensite phases. There are numerous advantages to establishing the material performance in advance of the lengthy experimental procedures with simulations to accelerate the understanding of these alloys and to establish a number of key properties. Therefore, rapid assessment of potential alloys can be ascertained via determination of twinning, slip and phase transformation barriers, the stability of different phases (austenite and martensite), their respective elastic constants, and lattice constants. In this paper

* Corresponding author.
E-mail address: huseyin@illinois.edu (H. Sehitoglu).

0749-6419/$ - see front matter © 2013 Elsevier Ltd. All rights reserved.
http://dx.doi.org/10.1016/j.ijplas.2013.08.017

Please cite this article in press as: Wang, J., et al. Dislocation slip stress prediction in shape memory alloys. Int. J. Plasticity (2013), http://dx.doi.org/10.1016/j.ijplas.2013.08.017

we focus on the slip stress determination with simulations and compare the results to experiments. We combine the ab-initio calculations with a modified mesoscale Peierls–Nabarro based formulation to determine stress levels for slip in close agreement with experiments.

We utilize the Ni_2FeGa as an example system to illustrate our methodology and then show its applicability to the most important SMAs. The Ni_2FeGa alloys are a new class of shape memory alloys (SMAs) and have received significant attention because of high transformation strain magnitudes (>12% in tension and >6% in compression) and low temperature hysteresis. They also have the potential for magnetic actuation and high temperature shape memory (Hamilton et al., 2007; Omori et al., 2004). The magnetic actuation requires twinning at low stress magnitudes, and high temperature shape memory can only occur in the presence of considerable slip resistance. These alloys are proposed to be a good alternative to the currently studied ferromagnetic Ni_2MnGa-based SMAs due to their superior ductility in tension (Barandiarán et al., 2008; Oikawa et al., 2002; Sutou et al., 2004; Yu et al., 2009). There are several crystal structures identified in Ni_2FeGa (Hamilton et al., 2006a, 2007; Whang et al., 1998), which exhibits martensitic transformations from $L2_1$ cubic austenite to intermediate 10M/14M modulated monoclinic martensites, and finally to the $L1_0$ tetragonal martensite (Efstathiou et al., 2008; Hamilton et al., 2008; Masdeu et al., 2005; Sutou et al., 2004). However, one can get a single stage transformation from $L2_1$ to $L1_0$ as temperature is increased (Hamilton et al., 2007), also in the case of nano-pillars (Ozdemir et al., 2012), and upon aging treatment (Chumlyakov et al., 2012). Therefore, a study on the $L1_0$ martensite is both scientifically interesting and technologically relevant. The phase transformation of Ni_2FeGa has been experimentally observed and theoretically investigated using atomistic simulations (Efstathiou et al., 2008; Hamilton et al., 2006a; Martynov, 1995; Segui et al., 2005; Sehitoglu et al., 2012). The results show that the $L2_1$ austenite requires high stress levels for dislocation slip while undergoing transformation nucleation at much lower stress magnitudes (Sehitoglu et al., 2012). However, the plastic deformation of $L1_0$ martensite via dislocation slip has not been fully understood, although it is very important in understanding the shape memory performance.

Fig. 1 shows a schematic of the stress–strain curve of Ni_2FeGa at temperatures in the range 75° C to 300 °C where $L2_1$ can directly transform to $L1_0$. These temperatures are significantly above the austenite finish temperature. The initial phase of Ni_2FeGa is $L2_1$ and it transforms to $L1_0$ when the stress level reaches the transformation stress. The transformation occurs at a near plateau stress followed by elastic deformation of martensite. With further deformation, dislocation slip (of $L1_0$) takes place at a critical stress designated as σ_{slip}. This stress is much higher than the transformation stress. During unloading, the reverse phase transformation occurs with plastic (residual) strain remaining in Ni_2FeGa as part of the deformation cannot be recovered.

It is well known that plastic deformation occurs via dislocation glide; and at the atomic level, dislocation glide occurs upon shear of atomic layers relative to one another in the lattice. At the dislocation core scale, quantum mechanics describe the atomic level interactions and the forces exerted on atoms; while at the mesoscale level, elastic strain fields of defects address the interactions (Kibey, 2007). The ensemble of dislocations and their interactions with the microstructure define the continuum behavior.

With atomistic simulations one can gain a better understanding of the lattice parameters and the unstable fault energies of $L1_0$. Therefore, atomistic simulations in this case will provide additional insight into material's behavior and the deformation mechanisms (Ezaz et al., 2011). Fig. 2 shows the different length scales associated with plasticity of transforming Ni_2FeGa alloys. The generalized stacking fault energy (GSFE) surface (γ-surface) at the atomic level (via atomistic simulations using density functional theory (DFT)) is shown at the lowest length scale. Of particular interest is the (1 1 1) plane, and from

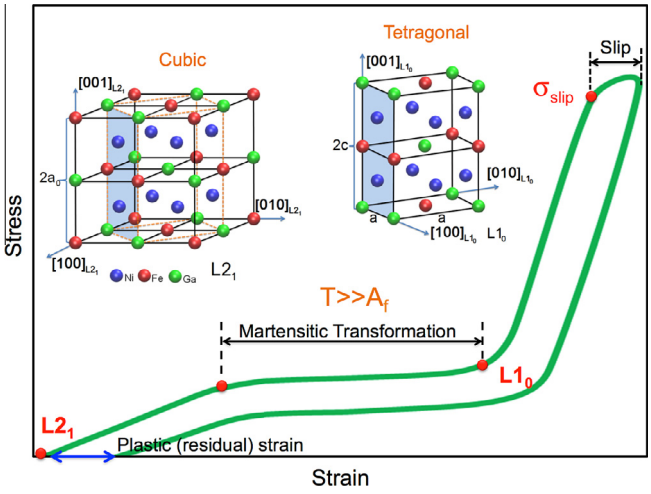

Fig. 1. Schematic illustration of the stress–strain curve showing the martensitic transformation from $L2_1$ to $L1_0$, and the dislocation slip in $L1_0$ of Ni_2FeGa at elevated temperature. After unloading, plastic (residual) strain is observed in the material as deformation cannot be fully recovered.

Please cite this article in press as: Wang, J., et al. Dislocation slip stress prediction in shape memory alloys. Int. J. Plasticity (2013), http://dx.doi.org/10.1016/j.ijplas.2013.08.017

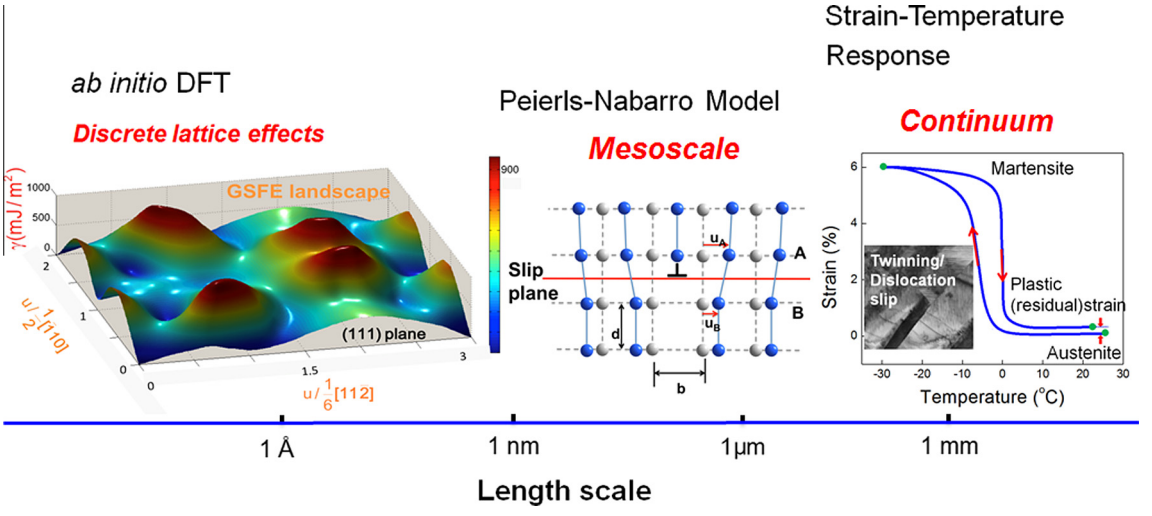

Fig. 2. Schematic description of the different length scales associated with plasticity in Ni_2FeGa alloys.

the entire γ-surface the propensity of slip in multiple directions can be established. The energy landscape for slip that is calculated is rather complex for the case of ordered shape memory alloys resulting in complex faults and anti-phase boundaries.

In the material science and meso-contiunuum mechanics field, coupling the various length scales involved in order to understand the plastic deformation still remains a major challenge (McDowell, 2010). The Peierls–Nabarro (P–N) model represents a mesoscale level integration of atomistic and elasticity theory considerations. It accounts for the dislocation cores on one hand and lattice resistance to flow by applying continuum concepts to elastic deformation at the atomic scale (Kibey, 2007). The model has stood the test of time over many years, and its main contribution is that the P–N stress level for dislocation glide is much lower than ideal stress calculations (Carrez et al., 2006; Hartford et al., 1998; Nabarro, 1947; Peierls, 1940). The calculations for P–N stress represent the breakaway of atoms within the core region of the dislocation. If the core is narrow the stress required to overcome the barrier is higher compared to the case of a wider core, and smaller Burgers vectors require lower stress for glide. Different slip systems in fcc, bcc and ordered crystals can be evaluated, and the most favorable planes and directions can be readily identified. Thus, the P–N model predicts stresses for dislocation slip more precisely than the theoretical shear strength obtained directly from atomistic simulations.

In this study, the P–N model with modifications will be utilized to study the slip resistance. In Fig. 2, the disregistry above and below the slip plane is shown which will be explained later in the paper. This results in a solution for the slip distribution (disregistry) within the core that exhibits a non-monotonic variation as a function of core position. We have made observations of slip during experiments in this paper and also in pseudoelasticity experiments at constant temperature. The dislocation slip was identified upon heating–cooling within the transformation electron microscopy (TEM) via in-situ observations. Finally, we compared the calculated slip stresses with experimental measurements of slip stress under compression loading to strain exceeding 6%. The agreement is excellent considering the complexity of real microstructures and the idealizations adopted in theoretical models.

The occurrence of dislocation slip is noted at the macro-scale by observing non-closure of the strain-temperature curves in Fig. 2. For example, upon cooling the austenite reverts to martensite and upon heating the reverse transformation occurs. If the entire process is reversible, the transformation strain in forward and reverse directions is identical. If plastic deformation develops, there is a residual strain upon heating to austenite. We are not attempting to predict the entire strain-temperature response at the continuum level (shown in Fig. 2) because multiple slip-twin systems and multi-phase interactions are governing. Our purpose is to point out the complexity of an isolated mechanism, mainly the dislocation glide behavior that contributes to the irreversibility.

1.2. Dislocation slip mechanism

So far, the investigation of $L1_0$ Ni_2FeGa martensite has been mostly through experimental research. Its properties are not well understood although it is very important to establish its dislocation slip behavior. The $L1_0$ Ni_2FeGa has a tetragonal structure with no modulation (Hamilton et al., 2008; Sutou et al., 2004). The modulation refers to the internally sheared crystal structures with periodic displacements. As a fundamental deformation mechanism, dislocation slip plays a critical role in defining the mechanical properties of SMAs, especially their irreversibility of transformation (Ezaz et al., 2013; Gall and Maier, 2002; Sehitoglu et al., 2012). It is likely that the material can exhibit different dislocation slip modes (planes and directions), which are activated at different stress levels. To quantitatively understand the experimentally observed dislocation slip, a detailed study via atomistic simulations is needed to determine active slip systems and compare with experimental findings. It is possible to investigate the dislocation slip via generalized stacking fault energy (GSFE) curves. GSFE is the

Please cite this article in press as: Wang, J., et al. Dislocation slip stress prediction in shape memory alloys. Int. J. Plasticity (2013), http://dx.doi.org/10.1016/j.ijplas.2013.08.017

interplanar potential energy determined by rigidly sliding one half of a crystal over the other half (Hartford et al., 1998; Lu et al., 2000). It was first introduced by Vitek (1968) and is a comprehensive definition of the fault energy associated with dislocation motion (Sehitoglu et al., 2012). By taking the maximum slope of the GSFE curve, the theoretical shear strength of the lattice along the slip direction is obtained. This stress is the upper bound on the flow stress of materials (Carrez et al., 2006; Joós and Duesbery, 1997) and is a much larger value compared to the experiments.

The Peierls–Nabarro (P–N) model is essentially based on continuum mechanics applied to lower length scales and addresses the dislocation structure by applying the elasticity theory and energetics from atomistic simulations. This model calculates stresses for dislocation slip more precisely. The corresponding Peierls stress τ_p is the minimum external stress required to move a dislocation irreversibly through a crystal and can be considered as the critical resolved shear stress at 0 K (Cordier et al., 2012; Wang et al., 2001; Wheeler et al., 2013). The slip system with lowest τ_p will be the dominant system in the crystal (Lu et al., 2000; Miranda and Scandolo, 2005; Nabarro, 1997). Recently, there has been renewed interest in calculating Peierls stress of dislocation by applying the P–N model (Lu et al., 2000; Schoeck, 1999). This is motivated by the advance of reliable first-principles calculations using DFT to determine the GSFE (γ energy) landscapes. However, when the GSFE curve comprises of multiple minima corresponding to various fault configurations, it cannot be approximated well by a single sinusoidal function as used in the original P–N model. Therefore, the representation of the P–N model needs to be modified to consider this complexity, which is described in detail in this study and applied for the dislocation slip calculations in $L1_0$ Ni_2FeGa.

1.3. Purpose and scope

A fundamental understanding of the dislocation slip that plays a key role in the shape memory behavior of $L1_0$ Ni_2FeGa is currently lacking, which is essential for understanding the mechanical response. Four possible slip systems in $L1_0$ martensite, $\frac{1}{2}\langle\bar{1}\,0\,1\rangle(1\,1\,1)$, $\frac{1}{2}\langle\bar{1}\,1\,0\rangle(1\,1\,1)$ $\frac{1}{6}\langle\bar{2}\,1\,1\rangle(1\,1\,1)$ and $\frac{1}{6}\langle1\,1\,\bar{2}\rangle(1\,1\,1)$ are considered in Ni_2FeGa. Three related types of planar defects, superlattice intrinsic stacking fault (SISF), complex stacking fault (CSF) and anti-phase boundary (APB), are analyzed. We note that due to the tetragonality of the $L1_0$ lattice of Ni_2FeGa, the dislocation behavior of $\frac{1}{6}[1\,1\,\bar{2}]$ is different from $\frac{1}{6}[\bar{2}\,1\,1]$ (similarly, $\frac{1}{2}[\bar{1}\,0\,1]$ is different from $\frac{1}{2}[\bar{1}\,1\,0]$), which results in different energy levels as reported in Section 3.2. Thus, in this paper the Miller indices with mixed parentheses $\langle u\,v\,w]$ and $\{h\,k\,l)$ are used in order to differentiate the first two equivalent indices (corresponding to the a and b axis in the $L1_0$ lattice) from the third (corresponding to the tetragonal c axis), which indicate that all permutations of the first two indices are allowed, whereas the third one is fixed (Appel et al., 2011). The purpose of this paper is to investigate the possible slip systems existing in $L1_0$ Ni_2FeGa, and to determine the most likely one by calculating the Peierls stresses and compare it with experimental observations. The results indicate that the mobility of the $\frac{1}{6}[1\,1\,\bar{2}]$ partial dislocation in the slip plane $(1\,1\,1)$ is controlling the plasticity of $L1_0$ Ni_2FeGa.

2. DFT calculation setup

We utilized DFT to precisely determine the undeformed and deformed energy states of $L1_0$ Ni_2FeGa during shearing in certain slip systems. The first-principles total-energy calculations were carried out using the Vienna ab initio Simulations Package (VASP) with the projector augmented wave (PAW) method and the generalized gradient approximation (GGA) (Kresse and Furthmuller, 1996; Kresse and Hafner, 1993). Monkhorst Pack $9 \times 9 \times 9$ k-point meshes were used for the Brillouin-zone integration to ensure the convergence of results. An energy cut-off of 500 eV was used for the plane-wave basis set. The total energy was converged to less than 10^{-5} eV per atom. We have used an n-layer based cell to calculate fault energies to generate GSFE curves in the different slip systems. We assessed the convergence of the GSFE energies with respect to increasing n, which indicates that the fault energy interaction in adjacent cells due to periodic boundary conditions will be negligible. The convergence is ensured once the energy calculations for n and $n+1$ layers yield the same GSFE. In the present work, n was taken as 10 in order to obtain the convergent results. For each shear displacement u, a full internal atom relaxation, including perpendicular and parallel directions to the fault plane, was allowed for minimizing the short-range interaction between misfitted layers near to the fault plane. This relaxation process caused a small additional atomic displacement r ($|r| = \sqrt{r_x + r_y + r_z}$) in magnitude within 1% of the Burgers vector b. Thus, the total fault displacement is not exactly equal to u but involves additional r. The total energy of the deformed (faulted) crystal was minimized during this relaxation process through which atoms can avoid coming too close to each other during shear (Fu and Yoo, 1992; Juan and Kaxiras, 1996; Paidar, 1976). From the calculation results of dislocation slip, we note that the energy barrier after full relaxation was near 10% lower than the barrier where the relaxation of only perpendicular to the fault plane was allowed.

3. Simulation results and discussion

3.1. The $L1_0$ crystal structure

We note that two different unit cells are used in literature to describe the $L1_0$ crystal structure. One is directly derived from the $L2_1$ body centered cubic (bcc) axes forming a body centered tetragonal (bct) structure (Fig. 3a); the other one is

Please cite this article in press as: Wang, J., et al. Dislocation slip stress prediction in shape memory alloys. Int. J. Plasticity (2013), http://dx.doi.org/10.1016/j.ijplas.2013.08.017

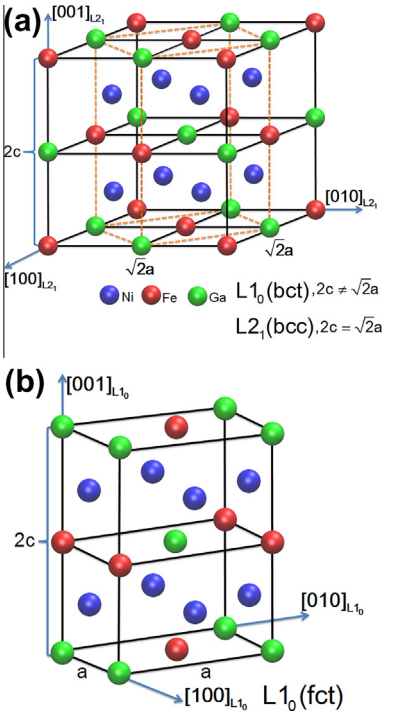

Fig. 3. $L1_0$ unit cell of Ni_2FeGa. (a) The body centered tetragonal (bct) structure of $L1_0$ is constructed from eight bct unit cells and has lattice parameters $\sqrt{2}a$, $\sqrt{2}a$ and $2c$. The blue, red and green atoms correspond to Ni, Fe and Ga atoms, respectively. The Fe and Ga atoms are located at corners and Ni atoms are at the center. The fct structure shown in brown dashed lines is constructed from the principal axes of $L1_0$. (b) The fct structure of $L1_0$ with lattice parameters a, a and $2c$ contains two fct unit cells. (For interpretation of the references to color in this figure legend, the reader is referred to the web version of this article.)

constructed from the principal axes of $L1_0$ forming the face centered tetragonal (fct) structure (shown in brown dashed lines in Fig. 3a). We note that if $2c = \sqrt{2}a$, Fig. 3a represents the $L2_1$ cubic structure; while if $2c \neq \sqrt{2}a$, it is the $L1_0$ tetragonal structure. In this paper, the $L1_0$ fct structure is considered and its corresponding lattice parameters are shown in Fig. 3b. Note that the tetragonal axis is $2c$, so the $L1_0$ unit cell contains two fct unit cells.

The lattice parameter of $L2_1$ cubic was calculated as $2a_o$ = 5.755 Å in our previous study (Sehitoglu et al., 2012). During the martensitic transformation from $L2_1$ cubic to $L1_0$ tetragonal in Ni_2FeGa, the unit cell volume can be changed since the material is always energetically more stable with lower energy level. For a certain unit cell volume of $L1_0$ tetragonal, there are many combinations of parameters c and a (or tetragonal ratio c/a), and one of these ratios yields the structure with the minimum energy level. To compute the unit cell volume change ΔV during the martensitic transformation, we considered a series of values $\Delta V/V_0$ (−3% to 3%), where V_0 is the $L2_1$ unit cell volume as the reference. For any $\Delta V/V_0$, we changed the tetragonal ratio c/a from 0.55 to 1.1 and found that the minimum crystal structural energy almost always remains at a c/a ratio of 0.95. The crystal structural energy as a function of c/a in varying $\Delta V/V_0$ was calculated and is shown in Fig. 4(a) (only a part of the calculated curves for a series of $\Delta V/V_0$ is shown for clarity). The lowest energy level among a series of $\Delta V/V_0$ was found at a $\Delta V/V_0$ of −0.76% and the corresponding crystal structure was $L1_0$. Fig. 4(b) is a high resolution plot of the red dashed lines in (a) showing the minimum energy level at the c/a ratio of 0.95 in the volume change $\Delta V/V_0$ of −0.76%. This energy was lower than $L2_1$ by 12.4 meV/atom, which indicates that the $L1_0$ is energetically more stable. The $L1_0$ lattice parameters were calculated as $a = b$ = 3.68 Å, and c = 3.49 Å in Table 1 and they were in a good agreement with experimental measurements (Sutou et al., 2004). We note that the alloy in the experiment is off stoichiometry ($Ni_{54}Fe_{19}Ga_{27}$) [2] compared to our simulations ($Ni_{50}Fe_{25}Ga_{25}$), which causes the slight difference of the lattice parameters. These precisely determined lattice parameters form the foundation of atomistic simulations in this study. In the following section, we establish GSFE curves based on these parameters.

3.2. Dislocation slip of $L1_0$ Ni_2FeGa

From the classical dislocation theory, the most favorable slip systems should contain the close-packed lattice planes and the Burgers vectors with shortest shear displacements. Thus, dislocation slip in the $L1_0$ fct structure favors the {1 1 1} planes along close or relatively close packed directions. The {1 1 1} planes are preferred planes as in fcc metals (Appel et al., 2011), but the favorable dislocations in these planes are not identified. It is well known that superdislocations of the $L1_0$ structure

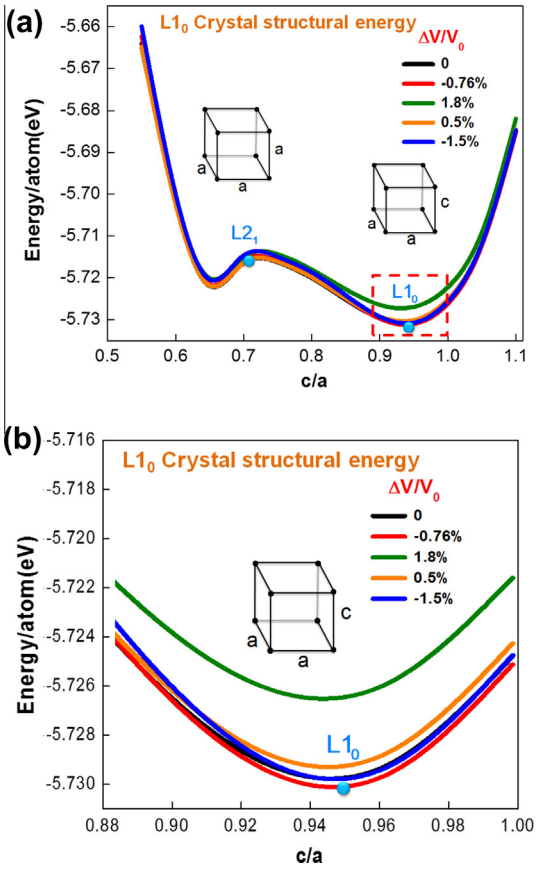

Fig. 4. (a) Crystal structural energy variation with tetragonal ratio c/a for a series of unit cell volume changes $\Delta V/V_0$, where $L2_1$ is considered as the reference volume V_0. The $L1_0$ tetragonal structure was found at a c/a of 0.95 for $\Delta V/V_0$ of −0.76%. (b) High resolution plot corresponding to the red dashed lines in (a). (For interpretation of the references to color in this figure legend, the reader is referred to the web version of this article.)

Table 1
VASP-PAW-GGA calculated $L1_0$ tetragonal lattice parameters, unit cell volume change $\Delta V/V_0$ and structural energy relative to $L2_1$ cubic in Ni_2FeGa compared with experimental data.

$L1_0$ tetragonal structure		Experiment (Sutou et al., 2004)	Theory (this study)
Lattice parameter (Å)	a	3.81	3.68
	c	3.27	3.49
Volume change $\Delta V/V_0$ (%)		−0.65	−0.76
Structural energy relative to $L2_1$ (meV/atom)		–	−12.4

The dash indicates that experimental data were not available for comparison.

can split into different types of partial dislocations with smaller Burgers vectors and smaller planar fault energies (Ehmann and Fähnle, 1998; Liu et al., 2007; Paidar, 2004). Fig. 5 shows a top view from the direction perpendicular to the (1 1 1) slip plane with three-layers of atoms stacking in $L1_0$ Ni_2FeGa. Four dislocations in this plane are presented: superdislocations $[\bar{1}\,1\,0]$, $\frac{1}{2}[1\,1\,\bar{2}]$ and $[\bar{1}\,0\,1]$, and partial dislocations, $\frac{1}{6}\langle\bar{2}\,1\,1\rangle$. Three types of planar defects, SISF (superlattice intrinsic stacking fault), CSF (complex stacking fault) and APB (anti-phase boundary) are marked on certain positions. We note that due to the non-unity tetragonal ratio c/a of 0.95, the $\frac{1}{6}[\bar{2}\,1\,1]$ dislocation vector is slightly larger (by 1.03) compared to $\frac{1}{6}[1\,1\,\bar{2}]$. The super-dislocation can split into the related Shockley partials, according to the dislocation reaction:

$$[\bar{1}10]=\frac{1}{6}[\bar{2}11]+\mathrm{CSF}+\frac{1}{6}[\bar{1}2\bar{1}]+\mathrm{APB}+\frac{1}{6}[\bar{2}11]+\mathrm{CSF}+\frac{1}{6}[\bar{1}2\bar{1}] \quad (1)$$

$$[\bar{1}01]=\frac{1}{6}[\bar{1}\bar{1}2]+\mathrm{SISF}+\frac{1}{6}[\bar{2}11]+\mathrm{APB}+\frac{1}{6}[\bar{1}\bar{1}2]+\mathrm{CSF}+\frac{1}{6}[\bar{2}11] \quad (2)$$

Please cite this article in press as: Wang, J., et al. Dislocation slip stress prediction in shape memory alloys. Int. J. Plasticity (2013), http://dx.doi.org/10.1016/j.ijplas.2013.08.017

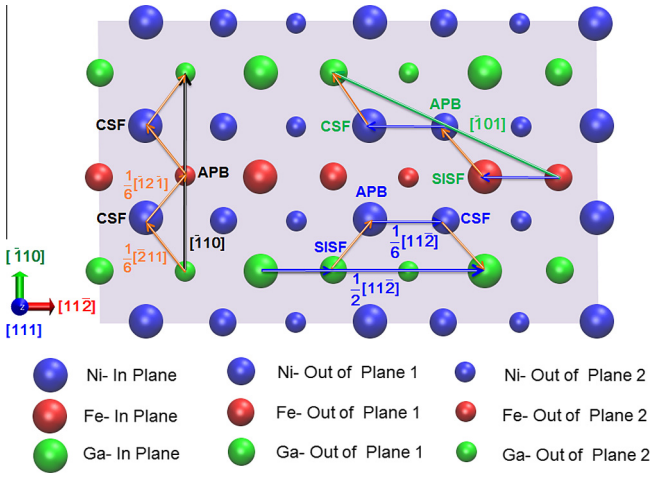

Fig. 5. Possible dislocations and atomic configurations of $L1_0$ Ni_2FeGa in the (1 1 1) plane. Different sizes of atoms represent three successive (1 1 1) layers from the top view. Dislocations $[\bar{1}\,1\,0]$, $\frac{1}{2}[1\,1\,\bar{2}]$, $[\bar{1}\,0\,1]$ and $\frac{1}{6}\langle\bar{2}\,1\,1\rangle$ are shown in different colors corresponding to Eqs. (1)–(3). Three types of planar defects, SISF CSF and APB are marked on certain positions.

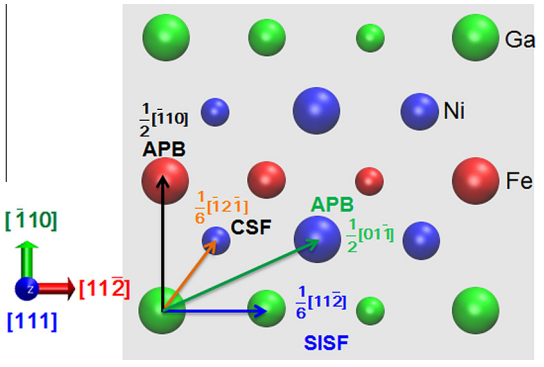

Fig. 6. Schematic of construction of slip movements that result in SISF, CSF and APB in the (1 1 1) plane.

$$\frac{1}{2}[11\bar{2}]=\frac{1}{6}[11\bar{2}]+\mathrm{SISF}+\frac{1}{6}[\bar{1}2\,\bar{1}]+\mathrm{APB}+\frac{1}{6}[11\bar{2}]+\mathrm{CSF}+\frac{1}{6}[2\,\bar{1}\,\bar{1}] \tag{3}$$

The different colors[1] in these equations correspond to Fig. 5 and represent the different dislocations and fault energies. We note that the superdislocation $\frac{1}{2}[1\,1\,\bar{2}]$ in Eq. (3) cannot be divided into three equal $\frac{1}{6}[1\,1\,\bar{2}]$ partials due to a much higher energy barrier (the detailed analysis is in Appendix A).

The planar defects SISF, CSF and APB are defined by pure movement of one half of a crystal over the other half in the (1 1 1) plane. The movement forms metastable positions corresponding to local minimum energies, which govern the dislocation slip behavior of $L1_0$ Ni_2FeGa. Fig. 6 shows a schematic of the construction of SISF, CSF and APB in the (1 1 1) plane due to atom movements along different directions. As denoted earlier, the three different atom sizes indicate three (1 1 1) layers of atoms stacking. A SISF is produced, when the in-plane atoms and all atoms above are shifted along the Burgers vector $\frac{1}{6}[1\,1\,\bar{2}]$. This displacement results in a stacking sequence where the in-plane Ga atoms lie directly above the out-of-plane Ga atoms. A CSF is generated, when the in-plane atoms and all atoms above are shifted along the Burgers vector $\frac{1}{6}[\bar{1}\,2\,\bar{1}]$. This displacement results in a stacking sequence where the in-plane Ga atoms lie directly above the out-of-plane Ni atoms. An APB is formed when the in-plane atoms and all atoms above are shifted along the Burgers vector $\frac{1}{2}[\bar{1}\,1\,0]$ (or $\frac{1}{2}[1\,0\,\bar{1}]$). This displacement results in a stacking sequence where the in-plane Ga atoms lie directly above the in-plane Fe (or Ni) atoms.

The slip plane and directions of possible slip systems in $L1_0$ Ni_2FeGa are shown in Fig. 7. The slip plane (1 1 1) is shown in Fig. 7a (shaded violet), which is the same as in fcc metals. We note that if the tetragonal axis is denoted as c, not $2c$, the corresponding slip plane will be (1 1 2). Fig. 7b shows four dislocations $\frac{1}{2}[\bar{1}\,0\,1]$, $\frac{1}{2}[\bar{1}\,1\,0]$, $\frac{1}{6}[\bar{2}\,1\,1]$ and $\frac{1}{6}[1\,1\,\bar{2}]$ in the (1 1 1) plane with Burgers vectors 2.54 Å, 2.6 Å, 1.49 Å, and 1.45 Å, respectively. The non-unity tetragonal ratio c/a results in different Burgers vectors between $\frac{1}{2}[\bar{1}\,0\,1]$ and $\frac{1}{2}[\bar{1}\,1\,0]$, and $\frac{1}{6}[\bar{2}\,1\,1]$ and $\frac{1}{6}[1\,1\,\bar{2}]$.

[1] For interpretation of color in Eqs. (1)–(3), the reader is referred to the web version of this article.

Please cite this article in press as: Wang, J., et al. Dislocation slip stress prediction in shape memory alloys. Int. J. Plasticity (2013), http://dx.doi.org/10.1016/j.ijplas.2013.08.017

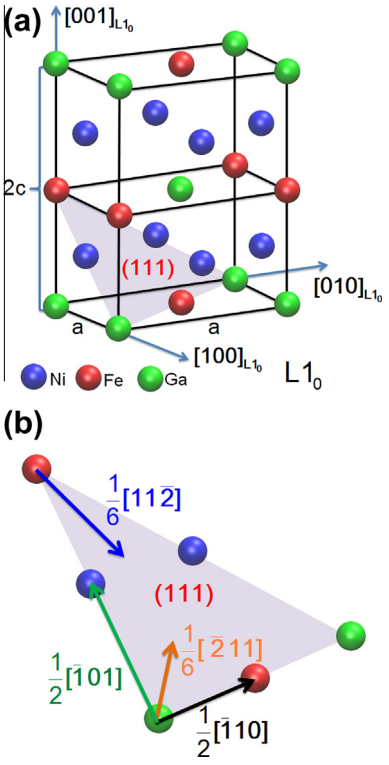

Fig. 7. Slip plane and dislocations of possible slip systems in $L1_0$ Ni_2FeGa. (a) The shaded violet area represents the slip plane (1 1 1) and (b) four dislocations $\frac{1}{2}[\bar{1}01]$, $\frac{1}{2}[\bar{1}10]$, $\frac{1}{6}[\bar{2}11]$ and $\frac{1}{6}[11\bar{2}]$ are shown in the (1 1 1) plane.

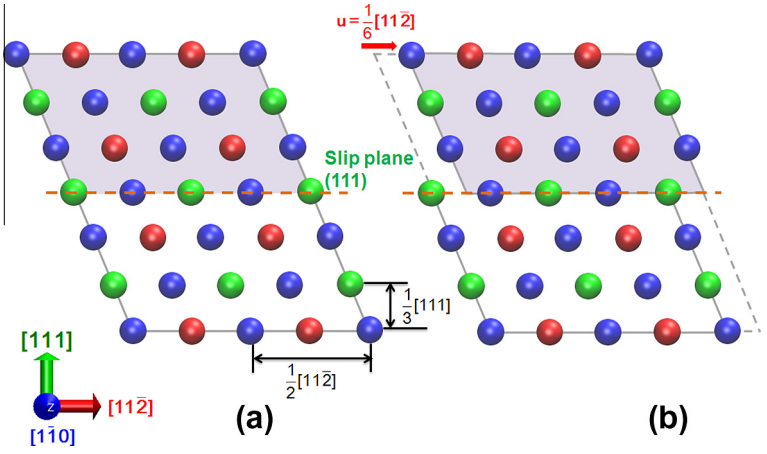

Fig. 8. Dislocation slip in the (1 1 1) plane with dislocation $\frac{1}{6}[11\bar{2}]$ of $L1_0$ Ni_2FeGa. (a) The perfect $L1_0$ lattice observed from the $[1\bar{1}0]$ direction. The slip plane (1 1 1) is marked with a brown dashed line. (b) The lattice after a rigid shear with dislocation $\frac{1}{6}[11\bar{2}]$, u, shown in a red arrow. (For interpretation of the references to color in this figure legend, the reader is referred to the web version of this article.)

The dislocation slip energy barriers and the faults (SISF, CSF and APB) are all characterized by the GSFE curve, which is calculated while one elastic half crystal is translated relative to the other in the slip plane along the slip direction (Ezaz et al., 2011). The $\frac{1}{6}[11\bar{2}](111)$ case of $L1_0$ Ni_2FeGa is illustrated in Fig. 8 showing the configuration of slip in the plane (1 1 1) with dislocation $\frac{1}{6}[11\bar{2}]$. Fig. 8a is the perfect $L1_0$ lattice before shear, while Fig. 8b is the lattice after shear by one Burgers vector, $u = \frac{1}{6}[11\bar{2}]$ (1.45 Å), in the slip plane.

All fault energies can be computed as a function of shear displacement u and are determined relative to the energy of the undeformed $L1_0$. The calculated shear displacements for the slip systems $\frac{1}{2}[\bar{1}01](111)$, $\frac{1}{2}[\bar{1}10](111)$, $\frac{1}{6}[\bar{2}11](111)$ and $\frac{1}{6}[11\bar{2}](111)$ were normalized by their respective Burgers vectors, and the corresponding GSFE curves are shown in Fig. 9.

Please cite this article in press as: Wang, J., et al. Dislocation slip stress prediction in shape memory alloys. Int. J. Plasticity (2013), http://dx.doi.org/10.1016/j.ijplas.2013.08.017

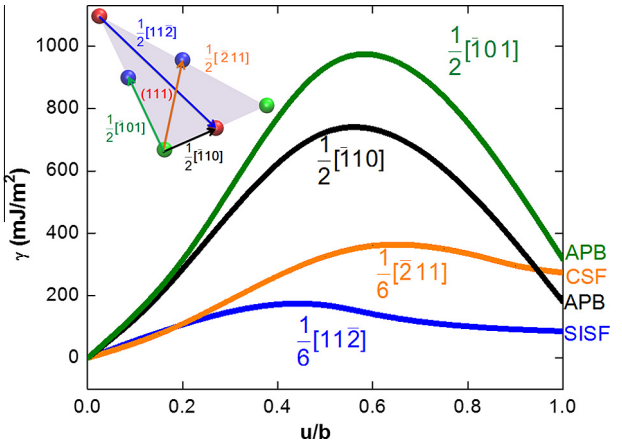

Fig. 9. GSFE curves (initial portion for one Burgers vector only) of $\frac{1}{2}[\bar{1}01]$, $\frac{1}{2}[\bar{1}10]$, $\frac{1}{6}[\bar{2}11]$ and $\frac{1}{6}[11\bar{2}]$ dislocations in the (111) plane of $L1_0$ Ni_2FeGa. The calculated shear displacement, u, was normalized by the respective Burgers vector, b.

We note that the dislocation $\frac{1}{2}[\bar{1}01]$ possesses the highest energy barrier of 932 mJ/m^2 (APB, 316 mJ/m^2). For the other three dislocations, the energy barriers decrease in the sequence of $\frac{1}{2}[\bar{1}10]$, $\frac{1}{6}[\bar{2}11]$ and $\frac{1}{6}[11\bar{2}]$, corresponding to 723 mJ/m^2 (APB, 179 mJ/m^2), 360 mJ/m^2 (CSF, 273 mJ/m^2) and 168 mJ/m^2 (SISF, 85 mJ/m^2), respectively.

The generalized stacking fault energy surface (γ surface) describes the energy variation when one half of a crystal is rigidly shifted over the other half with different fault vectors lying in a given crystallographic plane. To determine the γ surface corresponding to the DFT derived γ curves shown in Fig. 9, we chose a fourth order cosine-sine polynomial (Liu and Johnson, 2009), which can appropriately represent the energy variation in the (111) plane, i.e.

$$\gamma(k_1,k_2)=\sum_{m,n=0}^{m+n\leq 4} a_{mn}[X(k_1)]^m[X(k_2)]^n[1-\delta_{m0}\delta_{n0}]+\sum_{m,n=1}^{m+n\leq 4} b_{mn}[X(k_1)]^m[Y(k_2)]^n \tag{4}$$

where k_1 and k_2 are coefficients for fault vectors e in the (111) plane and $e = k_1e_1 + k_1e_1$, where $e_1=\frac{1}{6}[11\bar{2}]$ and $e_2=\frac{1}{2}[\bar{1}10]$ are unit vectors along the $[11\bar{2}]$ and $[\bar{1}10]$ directions, respectively. $[X(x)]=[1-\cos(\pi x)]$ and $[Y(x)]=[\sin(\pi x)]$. δ_{ij} represents Kronecker's delta (δ_{ij} is 1(0) if i is (not) equal to j). Fig. 10(a) shows the γ surface for the (111) plane of $L1_0$ Ni_2FeGa with the x axis along the $[11\bar{2}]$ direction, and the y axis along $[\bar{1}10]$. Fig. 10(b) is a two-dimensional projection of the γ surface in the (111) plane.

3.3. Peierls–Nabarro model for dislocation slip

The original P–N framework is based on a simple cubic crystal containing a dislocation with Burgers vector b shown in Fig. 11(a). Glide of the dislocation with this Burgers vector leaves behind a perfect crystal. This approach yields a variation in the GSFE with a periodicity of b and thus the γ energy can be approximated by using a single sinusoidal function as seen next. To calculate the Peierls stress for dislocation slip, a potential energy of displacement associated with the dislocation movement, misfit energy $E^s_\gamma(u)$, must be determined. This energy depends on the position of the dislocation line, u, within a lattice cell and reflects the lattice periodicity, thus it is periodic (Joós et al., 1994; Ogata et al., 2005; Schoeck, 1999) as shown in Fig. 11(b). The misfit energy $E^s_\gamma(u)$ across the glide plane is defined as the sum of misfit energies between pairs of atomic planes and can be obtained from the GSFE at the local disregistry. With obtained dislocation profiles and considering the lattice discreteness, the $E^s_\gamma(u)$ can be expressed as follows (Juan and Kaxiras, 1996):

$$E^s_\gamma(u)=\sum_{m=-\infty}^{+\infty}\gamma(f(ma'-u))a' \tag{5}$$

Where a' is the periodicity of $E^s_\gamma(u)$ and defined as the shortest distance between two equivalent atomic rows in the direction of the dislocation's displacement, $f(x)$ is the disregistry function representing the relative displacement (disregistry) of the two half crystals in the slip plane along the x direction, and u is the position of the dislocation line (Carrez et al., 2007; Joós and Duesbery, 1997; Lejček, 1973).By using the Frenkel expression (Tadmor and Miller, 2011), the $\gamma[f(x)]$ from GSFE can be written as follows:

$$\gamma[f(x)]=\frac{\gamma_{max}}{2}\left[1-\cos\frac{2\pi f(x)}{b}\right] \tag{6}$$

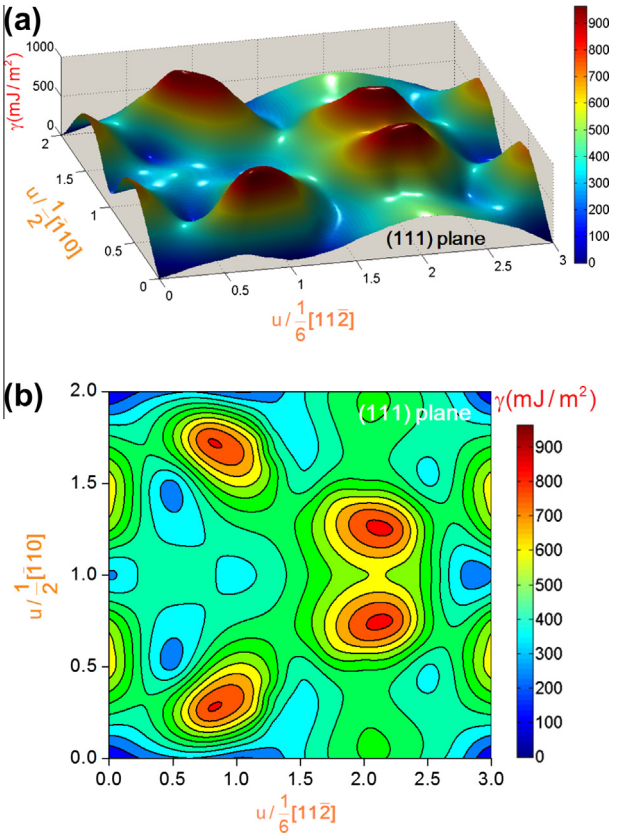

Fig. 10. (a) Generalized stacking fault energy surface (γ surface) for the (1 1 1) plane in $L1_0$ Ni_2FeGa. (b) A two-dimensional projection of the γ surface in the (1 1 1) plane. The x axis is taken along the [1 1 $\bar{2}$] direction, and y axis along [$\bar{1}$ 1 0].

where γ_{max} is the unstable stacking fault energy for GSFE, and b is the dislocation Burgers vector. Fig. 11(c) shows a schematic of $\gamma[f(x)]$ as a single sinusoidal function of $\frac{f(x)}{b}$.

The solution of the disregistry function $f(x)$ in the dislocation core is assumed to be of the Peierls type (Joós and Duesbery, 1997):

$$f(x) = \frac{b}{2} + \frac{b}{\pi}\arctan\left(\frac{x}{\zeta}\right) \tag{7}$$

where $\zeta = \frac{h}{2(1-\nu)}$ is the half-width of the dislocation for an isotropic solid (Joós et al., 1994), h is the interspacing between two adjacent slip planes and ν is Poisson's ratio. Fig. 11(d) shows the normalized $\frac{f(x)}{b}$ variation with $\frac{x}{\zeta}$.

After substituting Eqs. (6) and (7) into Eq. (5), we have the following formula of $E^s_\gamma(u)$:

$$E^s_\gamma(u) = \sum_{m=-\infty}^{+\infty}\gamma[f(ma'-u)]a' = \sum_{m=-\infty}^{+\infty}\frac{\gamma_{max}}{2}\left\{1+\cos\left[2tan^{-1}\left(\frac{ma'-u}{\zeta}\right)\right]\right\}a' \tag{8}$$

The Peierls stress τ_p is the maximum stress required to overcome the periodic barrier in $E^s_\gamma(u)$ and defined as the maximum slope of $E^s_\gamma(u)$ with respect to u (shown Fig. 11(d)) as follows:

$$\tau_p = max\left\{\frac{1}{b}\frac{dE^s_\gamma(u)}{du}\right\} \tag{9}$$

The Peierls stress τ_p is smaller than the theoretical shear strength $(\tau_{shear})_{nuc}$ and predicts experimental values more precisely. This is due to the fact that τ_p is determined not only by the energy barrier from GSFE curves, but also by the character of the dislocation slip distribution (Medvedeva et al., 1996). In this study, Peierls stresses of dislocation slip in $L1_0$ Ni_2FeGa were calculated based on the above equations. However, for the slip case of superdislocations dissociated to partial dislocations, the disregistry function $f(x)$ in Eq. (7) needs to be modified to include these partial dislocations with separation

Please cite this article in press as: Wang, J., et al. Dislocation slip stress prediction in shape memory alloys. Int. J. Plasticity (2013), http://dx.doi.org/10.1016/j.ijplas.2013.08.017

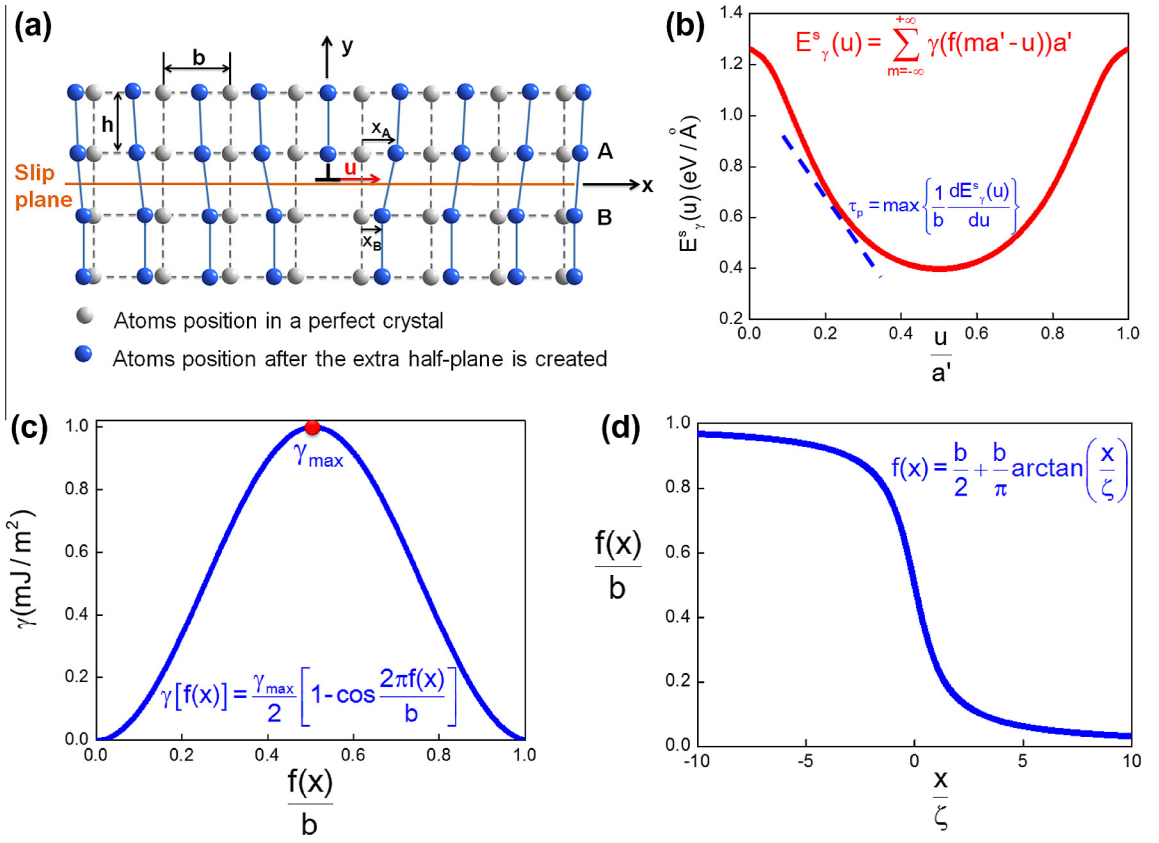

Fig. 11. Schematic illustration of Peierls–Nabarro model for dislocation slip. (a) A simple cubic crystal containing a dislocation with Burgers vector b. h is the interspacing between adjacent two slip planes. The relative displacement of the two half crystals in the slip plane along x direction, $x_A - x_B$, is defined as the disregistry function $f(x)$. (b) Schematic illustration showing the periodic misfit energy $E^s_\gamma(u)$ as a function of the position of the dislocation line, u. The Peierls stress τ_p is defined as the maximum slope of $E^s_\gamma(u)$ with respect to u. (c) Schematic showing the $\gamma[f(x)]$ energy (GSFE curve) as a single sinusoidal function of $\frac{f(x)}{b}$. (d) Schematic showing the normalized $\frac{f(x)}{b}$ variation with $\frac{x}{\zeta}$.

distances. Additionally, when the GSFE curve involves local minimum energy locations representing stacking faults, a single sinusoidal function in Eq. (6) cannot approximate it well and must be revised by applying multiple sinusoidal functions to fit it. The details of these modifications are described in Section 3.4.

3.4. Peierls stress calculations of $L1_0$ Ni_2FeGa

To determine the Peierls stresses required to move the dislocations, the misfit energies $E^s_\gamma(u)$ derived from GSFE curves must be calculated based on the method described in Section 3.3. However, for the case of GSFE curve comprising SISF, CSF and APB, the $E^s_\gamma(u)$ description is more complex than for simple fcc or bcc metals as a single sinusoidal function cannot approximate the GSFE curve well. Thus, revising the misfit energy formulation considering multiple sinusoidal functions to fit GSFE curves is necessary. For the case of the $[\bar{1}10]$ superdislocation dissociated into four partials with smaller Burgers vectors as given in Eq. (1), the GSFE curve is shown in Fig. 12.

The separations of the partial dislocations $d_1 = 0.538$ nm and $d_2 = 1.85$ nm are calculated by the condition that the force due to the surface tension of stacking faults balances the mutual repulsion of partials (Crawford et al., 1973; Sehitoglu et al., 2012; Stroh, 1958; Whelan et al., 1957) (calculation details in Appendix B). The disregistry function $f(x)$ can be described in Eq. (10) by considering the multiple partials, and Fig. 13 shows the normalized $\frac{f(x)}{b}$ variation with $\frac{x}{\zeta}$. In Fig. 13, d_1 and d_2 are the distances between partial dislocations, and their values depend on the CSF and APB:

$$f(x) = \frac{b}{\pi}\left[\arctan\left(\frac{x}{\zeta}\right) + \arctan\left(\frac{x-d_1}{\zeta}\right) + \arctan\left(\frac{x-(d_1+d_2)}{\zeta}\right) + \arctan\left(\frac{x-(2d_1+d_2)}{\zeta}\right)\right] + 2b \tag{10}$$

We note that this GSFE curve does not fit a single sinusoidal relation; instead, it is approximated by a sinusoidal series function. Thus, the corresponding misfit energy is presented as the explicit form in Eq. (11), and Fig. 14 shows the misfit energy $E^s_\gamma(u)$ variation with the lattice period a′. Two quantities $(E^s_\gamma)_{a'/2}$ and $(E^s_\gamma)_p$ in the plot are denoted. The $(E^s_\gamma)_{a'/2}$

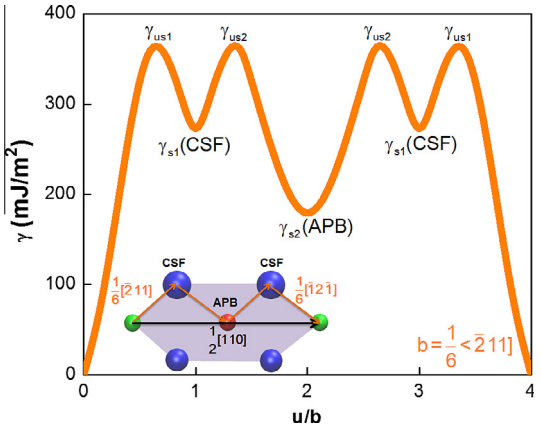

Fig. 12. Upon shearing the superdislocation $[\bar{1}\,1\,0]$, the dissociation into four partials and the associated CSF and APB energies are determined. The unstable stacking fault energies $\gamma_{us1} = \gamma_{us2} = 360$ mJ/m^2 (energy barriers); the stable stacking fault energies $\gamma_{s1} = 273$ mJ/m^2 (CSF) and $\gamma_{s2} = 179$ mJ/m^2 (APB).

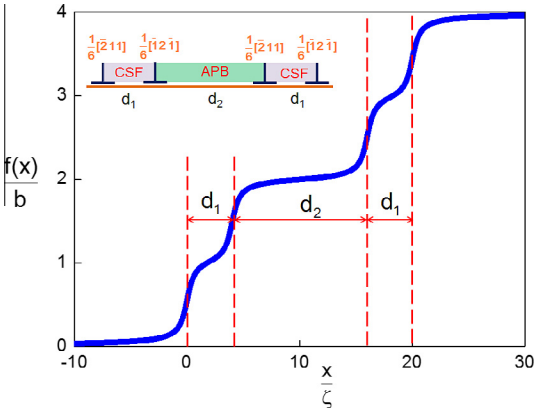

Fig. 13. The disregistry function $f(x)$ for the superdislocation $[\bar{1}\,1\,0]$ dissociated into four partials $\frac{1}{6}\langle\bar{2}\,1\,1]$. The separation distances of the partial dislocations are indicated by d_1 and d_2.

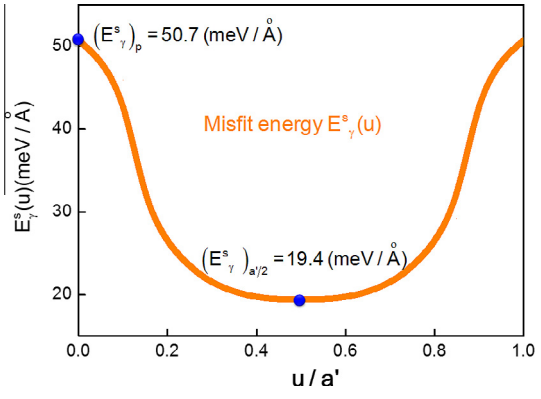

Fig. 14. Misfit energy $E^s_\gamma(u)$ for the superdislocation $[\bar{1}\,1\,0]$ dissociated into four partials $\frac{1}{6}\langle\bar{2}\,1\,1]$.

represents the minimum of $E^s_\gamma(u)$ function and provides an estimate of the core energy of dislocations. The $(E^s_\gamma)_p$ is defined as the Peierls energy, which is the amplitude of the variation of $E^s_\gamma(u)$ and the barrier required to move dislocations (Joós et al., 1994).

Please cite this article in press as: Wang, J., et al. Dislocation slip stress prediction in shape memory alloys. Int. J. Plasticity (2013), http://dx.doi.org/10.1016/j.ijplas.2013.08.017

Table 2
Calculated shear modulus, theoretical shear strength and Peierls stress for dislocation slip of $L1_0$ Ni_2FeGa.

Slip plane	Burgers vector, b	Shear modulus (GPa) $\mu = 2\pi(\tau_{shear})_{nuc}$	Theoretical shear stress (GPa) $(\tau_{shear})_{nuc} = max\{\frac{\partial\gamma}{\partial u}\}$	Critical shear stress (theory) – this study (GPa) $\tau_p = max\{\frac{1}{b}\frac{dE_\gamma^s(u)}{du}\}$
(1 1 1)	$\frac{1}{2}[\bar{1}\,0\,1]$	61.3	9.76	5.8
(1 1 1)	$\frac{1}{2}[\bar{1}\,1\,0]$	52.5	8.36	3.13
(1 1 1)	$\frac{1}{6}[\bar{2}\,1\,1]$	29.5	4.7	1.26
(1 1 1)	$\frac{1}{6}[1\,1\,\bar{2}]$	22.9	3.65	1.1

$$E_\gamma^s(u) = \sum_{n=1}^{6}(E_\gamma^s)_n(u) = \sum_{m=-\infty}^{0}\frac{\gamma_{us1}}{2}\left[1-\cos\frac{2\pi f(ma'-u)}{b}\right]a' + \sum_{m=1}^{\infty}\left\{\frac{\gamma_{us1}-\gamma_{s1}}{2}\left[1-\cos\frac{2\pi f(ma'-u)}{b}\right]\right\}a'$$
$$+ \sum_{m=-\infty}^{\infty}\left\{\frac{\gamma_{us2}-\left(\frac{\gamma_{s1}+\gamma_{s2}}{2}\right)}{2}\left[1-\cos\frac{2\pi f(ma'-u)}{b}\right]\right\}a' + \sum_{m=-\infty}^{\infty}\left\{\frac{\gamma_{us2}-\left(\frac{\gamma_{s1}+\gamma_{s2}}{2}\right)}{2}\left[1-\cos\frac{2\pi f(ma'-u)}{b}\right]\right\}a'$$
$$+ \sum_{m=-\infty}^{0}\left\{\frac{\gamma_{us1}-\gamma_{s1}}{2}\left[1-\cos\frac{2\pi f(ma'-u)}{b}\right]\right\}a' + \sum_{m=1}^{\infty}\frac{\gamma_{us1}}{2}\left[1-\cos\frac{2\pi f(ma'-u)}{b}\right]a' \quad (11)$$

Once the misfit energy is determined, the Peierls stress τ_p can be calculated by the maximum of $\frac{1}{b}\frac{dE_\gamma^s(u)}{du}$. As mentioned before, by taking the maximum slope of the GSFE curve, the theoretical shear strength $(\tau_{shear})_{nuc}$ for each slip system is obtained. The corresponding shear modulus μ can then be approximately determined as $\mu = 2\pi(\tau_{shear})_{nuc}$ (Hosford, 2005). The calculated shear modulus μ, theoretical shear strength $(\tau_{shear})_{nuc}$ and Peierls stress τ_p for the four slip systems of $L1_0$ Ni_2FeGa are shown in Table 2. We note that τ_p is smaller than $(\tau_{shear})_{nuc}$ and predicts experimental values more precisely, as described in Section 3.3. However, the theoretical shear strength $(\tau_{shear})_{nuc}$ follows the trend of the Peierls stress τ_p for these four slip systems.

Combining the results of $(\tau_{shear})_{nuc}$ and τ_p, we note that the $\frac{1}{6}[1\,1\,\bar{2}]$ has the lowest stress levels and will be most likely the first to activate. Both of the $\frac{1}{2}[\bar{1}\,1\,0]$ and $\frac{1}{2}[\bar{1}\,0\,1]$ dislocations possess significantly higher $(\tau_{shear})_{nuc}$ and τ_p values than $\frac{1}{6}[\bar{2}\,1\,1]$ and $\frac{1}{6}[1\,1\,\bar{2}]$, so these superdislocations will split into $\frac{1}{6}\langle 211\rangle$ partials and planar defects left between them as shown in Eqs. (1) and (2). However, when the Schmid factor associated with internal shear stresses provides a larger contribution, the glide of $\frac{1}{2}[\bar{1}\,0\,1]$ and $\frac{1}{2}[\bar{1}\,1\,0]$ superdislocations can also be activated. Thus, the Peierls stress calculated in combination with the P–N model and GSFE curves provides a basis for a theoretical study of the dislocation structure and operative slip modes in $L1_0$ Ni_2FeGa.

4. Experimental observations and viewpoints on martensite deformation behavior

4.1. In-situ TEM observations of dislocation slip

Understanding the dislocation slip behavior of shape memory alloys is extremely relevant to understanding the shape memory performance. The higher the resistance to martensite slip, the superior the shape memory performance.

During dynamic evolution of phase boundaries, both austenite and martensite may undergo slip due to the high internal stress fields. Because observations of slip are difficult to make during the loading experiments, one way to prepare the samples for such observations is to subject the specimens to phase change, remove the sample, and then conduct heating cooling experiments in an transmission electron microscope (TEM). The first portion of the experiment is sometimes referred to as training to obtain a two way shape memory effect. During this experiment one can transform the austenite to the $L1_0$ phase under stress and interrupt the experiment at room temperature, so one can retain the martensite $L1_0$ phase. Then, samples are cut from the $L1_0$ specimens, which are observed in the TEM. Cooling in the TEM further allows observations of the evolution of dislocation slip behaviors. Such experiments were conducted and the results confirm dislocation slip in the martensitic phase. To ensure that the resultant phase is the $L1_0$ phase and not the 10M/14M intermediate martensites, the stress is raised in a stair case fashion to sufficiently high levels, and diffraction peaks were collected to index the martensite $L1_0$ phase. When the stress is not sufficiently high (less than 40 MPa), the diffraction peaks corresponded to 14M, an intermediate martensitic structure. When the stress was 80 MPa, the final martensitic phase observed was $L1_0$. These results are shown in Figs. 15 and 16 for applied stress levels of 40 MPa and 80 MPa respectively.

At tensile stress of 40 MPa, the transformation steps were $L2_1 \rightleftharpoons 10M \rightleftharpoons 14M$ shown in Fig. 15. We note that the strain saturates at nearly 6.2% and the formation of 14M structure is confirmed with diffraction measurements at room temperature. The inset shows a selected area diffraction (SAD) pattern of the 14M structure.

When the tensile stress was increased to 80 MPa, the transformation steps (cooling) were $L2_1 \rightarrow 10M \rightarrow 14M \rightarrow L1_0$ shown in Fig. 16. The strain saturates approximately at 9.5% and the crystal structure is $L1_0$ at room temperature. The inset shows a SAD pattern of the $L1_0$ structure. Compared to the maximum strain of 6.2% in the transformation $L2_1 \rightleftharpoons 10M \rightleftharpoons 14M$ in Fig. 15, we note that once $14M \rightarrow L1_0$ forms, the $L1_0$ detwins in tension. Because the test is interrupted near room temperature the specimen has not reverted to the austenitic phase ($L2_1$). In the second phase of the experiments,

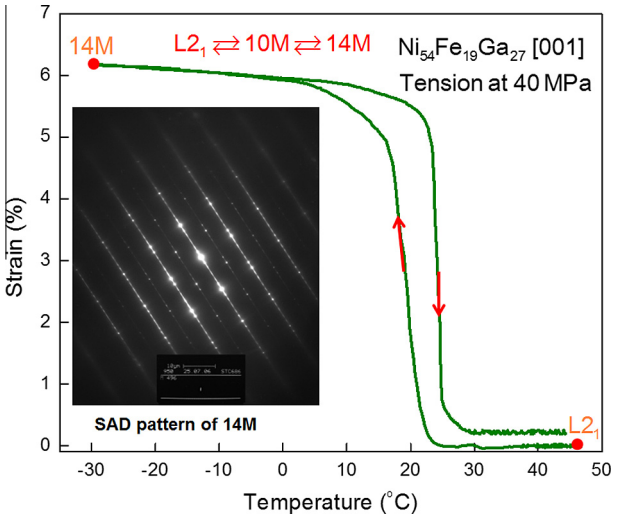

Fig. 15. The tensile strain-temperature response at 40 MPa describing the inter-martensitic transformation $L2_1 \rightleftharpoons 10\,M \rightleftharpoons 14\,M$. Red arrows along the curve indicate directions of cooling and heating. A SAD pattern is insetted showing the culmination in formation of the 14 M structure. (For interpretation of the references to color in this figure legend, the reader is referred to the web version of this article.)

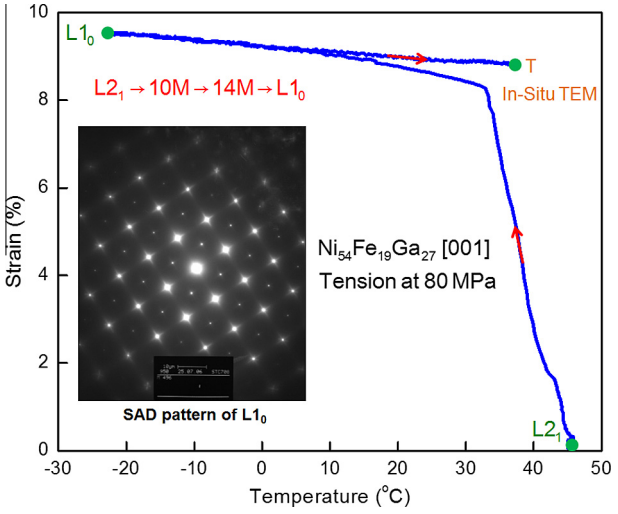

Fig. 16. The tensile strain-temperature response at 80 MPa indicating the martensitic transformation from the austenite $L2_1$ to the non-modulated martensite $L1_0$. A SAD pattern in the inset shows resulting $L1_0$ structure. The sample is removed from the load frame at 'T' and studied with TEM under in-situ temperature cycling.

the sample that is shown in Fig. 16 was subsequently studied by TEM via in-situ heating and cooling. The existence of dislocations slip of $L1_0$ at -6 °C is shown in Fig. 17.

4.2. Determination of martensite slip stress from experiments

Our previous compression experiments show that as the temperature increases to 150 °C, the austenite $L2_1$ can directly transform to $L1_0$ martensite bypassing the intermartensite 10M/14M (Hamilton et al., 2007). A series of experiments were conducted to study the martensite slip behavior ($L1_0$) subsequent to austenite to martensite transformation. These experiments involve compression loading of [001] oriented single crystals of $Ni_{54}Fe_{19}Ga_{27}$ at a constant temperature of 150 °C. A typical compressive stress–strain curve is shown in Fig. 18. The samples were originally in the $L2_1$ state and directly transformed to the $L1_0$ regime when the loading reached the martensitic transformation stress of 450 MPa. Upon further loading, the samples were in a fully $L1_0$ state and dislocation slip was observed as the stress magnitude exceeded 1500 MPa. After unloading, a finite amount of plastic strain remained due to residual dislocations in the $L1_0$. Because the [001] orientation in $L2_1$ corresponds to [001] in $L1_0$ (Fig. 3), the Schmid factor for the compressive axis [001] and dislocation slip system

Please cite this article in press as: Wang, J., et al. Dislocation slip stress prediction in shape memory alloys. Int. J. Plasticity (2013), http://dx.doi.org/10.1016/j.ijplas.2013.08.017

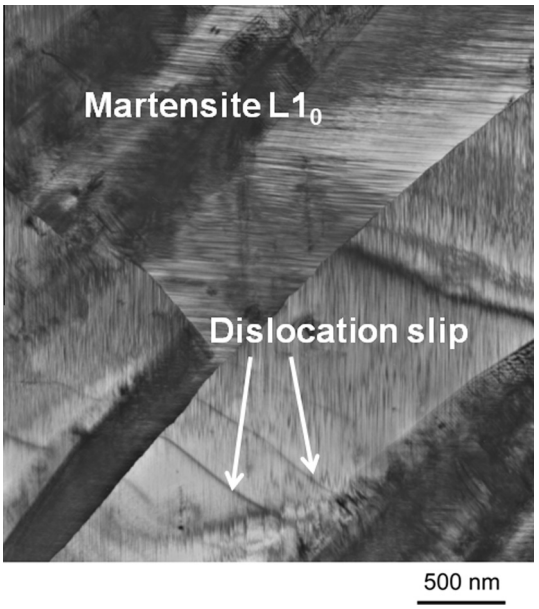

Fig. 17. Upon cooling to −6 °C, the TEM image displays the martensite phase $L1_0$ with $\langle 1\,1\,2\rangle\{1\,1\,1\}$ dislocation slip in a $Ni_{54}Fe_{19}Ga_{27}$ (at %) single crystal.

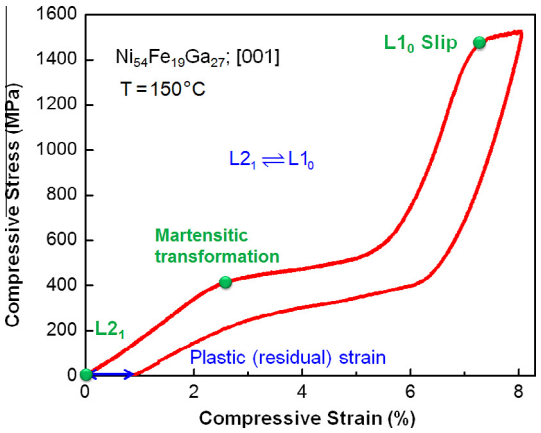

Fig. 18. Compressive stress–strain response of $Ni_{54}Fe_{19}Ga_{27}$ at a constant temperature of 150 °C.

Table 3
Comparison of experimental and predicted slip stress levels for $L1_0$ N_2FeGa.

Slip system	Crystal structure	Present theory (GPa)	Experiment (GPa)
$(1\,1\,1)\frac{1}{6}[1\,1\,\bar{2}]$	$L1_0$	1.1	0.7–1.0

$[1\,1\,\bar{2}](1\,1\,1)$ in $L1_0$ is near 0.5. The shear stress of dislocation slip in $L1_0$ at a temperature of 150 °C is then calculated as 750 MPa. We note that the Peierls stress is the shear stress required to move a dislocation at 0 K, where the thermal activation is absent and the dislocation moves only due to the influence of stress. On the other hand, at finite temperature, the dislocation movement can be assisted by both thermal activation and stress, and thus the shear stress for dislocation motion is lower than the one required at 0 K (Cordier et al., 2012; Wang, 1996). Therefore, our Peierls stress of 1.1 GPa can be compared with the experimental value of 750 MPa (Table 3); while the theoretical shear strength of 3.65 GPa is much higher than the experimental data. This verification demonstrates that the extended P–N formulation provides a useful and rapid prediction of the dislocation slip stress.

Please cite this article in press as: Wang, J., et al. Dislocation slip stress prediction in shape memory alloys. Int. J. Plasticity (2013), http://dx.doi.org/10.1016/j.ijplas.2013.08.017

Table 4
Predicted Peierls stresses for shape memory alloys are compared to known reported experimental values. The slip systems and crystal structures of SMAs are given. ($L2_1$ and B2 are the crystal structures in austenite phase.)

Material	Crystal structure	Slip system	Critical shear stress-present theory (GPa)	Critical shear stress-experiment (GPa)
Ni_2FeGa	$L2_1$	$(1\bar{1}0)\frac{1}{4}[111]$	0.63	0.40–0.65 (Timofeeva et al., 2012)
Co_2NiGa	B2	(011)[100]	0.76	0.40–0.70 (Chumlyakov et al., 2008b; Karaman and Lagoudas, 2006)
Co_2NiAl	B2	(011)[100]	0.72	0.60–0.80 (Chumlyakov et al., 2008b; Dilibal et al., 2011)
NiTi	B2	(011)[100] $(011)[1\bar{1}1]$	0.71 1.2	0.40–0.80 (Chumlyakov et al., 2008a; Efstathiou and Sehitoglu, 2008; Ezaz et al., 2013; Sehitoglu et al., 2001)
Ni_2TiHf	B2	(011)[100]	0.78	0.55–0.75 (Coughlin et al., 2012; Wang et al., 1999)
CuZn	B2	$(011)[1\bar{1}1]$	0.08	0.03–0.07 (Romero et al., 1988; Wollmershauser et al., 2009)

5. Prediction of dislocation slip stress for shape memory alloys

To validate the extended P–N formulation for dislocation slip, we calculated Peierls stresses predicted from the model for several important shape memory alloys in austenite phase and compared to the experimental slip stress data. The martensite slip stress levels are rather high as we show in this study (1.1 GPa versus 0.63 GPa). The austenite slip stress levels, on the other hand, are more readily available in the experiments and are also very important. The austenite of these materials (Ni_2FeGa, Co_2NiGa, Co_2NiAl, NiTi, CuZn and Ni_2TiHf) possess the $L2_1$ and B2 cubic structures. We found excellent agreement between the predicted values and experimental data shown in Table 4. For each material, the lattice type, the slip system, and the experimental range of critical slip stresses and the theory are shown. If the ideal stress levels are included, these exceed several GPa and are much higher than experiments. Interestingly, the critical stress for CuZn, which has excellent transformation properties, but suffers from plastic deformation, exhibits the lowest levels. For austenitic NiTi the most likely slip system is (011)[100] with a slip stress level of 0.71 GPa consistent with experiments.

The experimental slip stress data are taken from the plot of critical stress vs. temperature. In all the studied materials, a similar stress vs. temperature correlation is observed such that near the M_d temperature the material undergoes slip. The critical stress for martensitic transformation increases with temperature above A_f and the critical stress for dislocation slip of austenite decreases with temperature. When these two values cross at the temperature M_d, the stress-induced martensitic transformation is no longer possible, but the dislocation slip of austenite dominates the mechanical response. The critical austenite slip stress at M_d is considered as the relevant experimental data for austenite slip and compared to the (Peierls based) present theory.

6. Summary

The present work focuses on the dislocation slip mechanism of $L1_0$ Ni_2FeGa, and the rationalization of why $\frac{1}{6}[11\bar{2}]$ is the favorable dislocation slip system. The simulations underscore a significant quantitative understanding of Ni_2FeGa and extend the Peierls–Nabarro (P–N) formulation for the study of complex faults.

The calculated lattice parameters of $L1_0$ are in good agreement with the available experimental results, which form the foundation of the GSFE and Peierls stress calculation. We identified the energies and stresses required for dislocations movement of $L1_0$ Ni_2FeGa. To address this issue, we precisely established the GSFE curves and determined energy barriers and planar faults (SISF, CSF and APB) for possible dislocations, $\frac{1}{6}[11\bar{2}]$, $\frac{1}{6}[\bar{2}11]$, $\frac{1}{2}[\bar{1}10]$ and $\frac{1}{2}[\bar{1}01]$. The theoretical shear stresses $(\tau_{shear})_{nuc}$ were estimated from the maximum slope of the GSFE curves in Table 2. The $(\tau_{shear})_{nuc}$ forms the upper bound of the mechanical strength of the material and it is much higher than experimental results. Once the GSFE curves were established, the Peierls stresses τ_p were calculated based on the extended P–N model. The determination of misfit energy is rather complex and considers the presence of multiple partials.

We illustrated with the energy barrier and Peierls stress τ_p that $\frac{1}{6}[11\bar{2}]$ is preferred over other dislocations in $L1_0$ Ni_2FeGa. The slip system $\frac{1}{6}[11\bar{2}]$ (111) possesses the smallest barrier of 168 mJ/m^2 and corresponding Peierls stress of 1.1 GPa. We note that both of the superdislocations $\frac{1}{2}[\bar{1}10]$ and $\frac{1}{2}[\bar{1}01]$ can split into $\frac{1}{6}\langle 211\rangle$ partials while planar defects (SISF, CSF and APB) are formed during their dissociation process. However, we emphasize that the glide of $\frac{1}{2}[\bar{1}01]$ and $\frac{1}{2}[\bar{1}10]$ can also be activated at higher applied stress. In the present study, we performed a fully atomic relaxation to establish the GSFE, since unrelaxed GSFE does not represent the precise energy barrier in association with the dislocation glide. We compared unrelaxed and relaxed GSFE of slip system $\frac{1}{6}[11\bar{2}]$ (111) in $L1_0$ Ni_2FeGa. We note that the barrier for unrelaxed and relaxed GSFE is 180 mJ/m^2 and 168 mJ/m^2, respectively, which represents a 7% difference between these two values. The results reported in the paper are the relaxed values. The predicted Peierls stress is 1.15 GPa and 1.1 GPa, respectively, a near 5% difference. We

Please cite this article in press as: Wang, J., et al. Dislocation slip stress prediction in shape memory alloys. Int. J. Plasticity (2013), http://dx.doi.org/10.1016/j.ijplas.2013.08.017

note that the relaxed GSFE predicts a closer result to the experiments. Therefore, by allowing fully atomic relaxation, our GSFE is modified from the rigid shift condition (Clouet, 2012; Hartford et al., 1998a; Lu, 2005; Paidar, 1976; Tadmor and Miller, 2011).

We note that there are alternative approaches to determine the dislocation core by performing direct DFT (Clouet, 2012; Trinkle, 2008; Woodward, 2005; Woodward and Rao, 2002) calculations. These approaches confirm the accuracy of the disregistry function of the arctan form derived from the PN model (Clouet, 2012). For the case of superdislocation dissociated into four partials in the present study, further developments in the direct DFT approach are needed including modifications of the Lattice Green's functions (Trinkle, 2008).

To validate our Peierls stress prediction, we conducted a series of experiments to observe the dislocation slip in $L1_0$ Ni_2FeGa and determined the slip stress of $L1_0$ approximately as 1.5 GPa (CRSS is 750 MPa) under compression loading of [0 0 1] samples. The single crystals underwent slip deformation following austenite to martensite transformation. These results confirmed our Peierls stress prediction of 1.1 GPa for the $\frac{1}{6}[1\,1\,\bar{2}]$ (1 1 1) slip system. These predicted levels with the P–N model are in far better agreement with experiments in comparison with the theoretical stress level of 3.65 GPa. In addition to the temperature effects discussed earlier, some of the differences may stem from the fact that the actual alloy is off stoichiometry ($Ni_{54}Fe_{19}Ga_{27}$) compared to the simulations ($Ni_{50}Fe_{25}Ga_{25}$). The theoretical lattice constants are not exactly the same as the experimental values contributing to some of the differences in stress levels.

We also investigated dislocation slip in several important shape memory alloys and predicted stresses based on the present theory for Ni_2FeGa (austenite), NiTi, Co_2NiGa, Co_2NiAl, CuZn and Ni_2TiHf austenites in excellent agreement with experiments. Overall, we note that the stresses calculated with the extended P–N model and GSFE curves provides an excellent basis for a theoretical study of the dislocation structure and operative slip modes in $L1_0$ Ni_2FeGa and the some of the most important shape memory alloys. The formulation can be extended to other proposed shape memory alloys with different crystal structures as well.

Acknowledgments

The work was supported by the National Science Foundation, CMMI 09-26813. This support is gratefully acknowledged.

Appendix A. GSFE of $\frac{1}{2}[1\,1\,\bar{2}]$ dissociation into three $\frac{1}{6}[1\,1\,\bar{2}]$ partials

Similar to the dislocation dissociation in fcc metals (Kibey et al., 2006), it is very unlikely to dissociate the superdislocation $\frac{1}{2}[1\,1\,\bar{2}]$ into three $\frac{1}{6}[1\,1\,\bar{2}]$ partial dislocations, due to the much higher energy barrier formed when the atoms in the same plane slide past each other. We calculated the GSFE curve for the superdislocation $\frac{1}{2}[1\,1\,\bar{2}]$ dissociated into three $\frac{1}{6}[1\,1\,\bar{2}]$ partial dislocations in Fig. A1. After shearing with a displacement $u = \frac{1}{6}[1\,1\,\bar{2}]$, a metastable structure is obtained at point S in the curve. Similar to fcc metals (Kibey et al., 2006), further shear beyond point S along the $[1\,1\,\bar{2}]$ direction results in an unstable structure at point C ($u = \frac{1}{3}[1\,1\,\bar{2}]$). We note that this unstable stacking fault energy (global energy barrier) is 475 mJ/m^2, which is much higher than the energy barrier of 360 mJ/m^2 along the direction $\frac{1}{6}[\bar{1}\,2\,\bar{1}]$ shown in Fig. 12. Thus, it is impossible to dissociate the superdislocation $\frac{1}{2}[1\,1\,\bar{2}]$ into three $\frac{1}{6}[1\,1\,\bar{2}]$ partial dislocations; instead, it will dissociate into the combination of $\frac{1}{6}[1\,1\,\bar{2}]$ and $\frac{1}{6}[\bar{1}\,2\,\bar{1}]$ shown in Eq. (3).

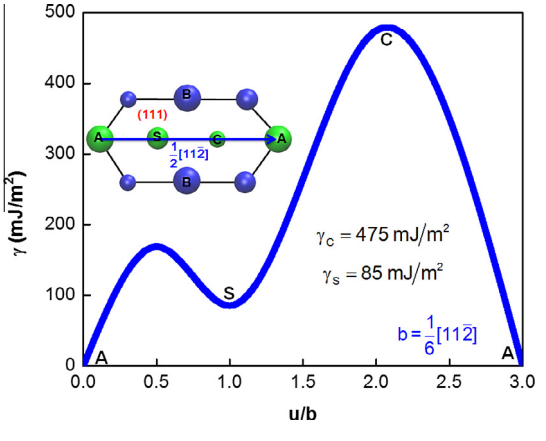

Fig. A1. GSFE curve of the superdislocation $\frac{1}{2}[1\,1\,\bar{2}]$ dissociated into three $\frac{1}{6}[1\,1\,\bar{2}]$ partial dislocations on the (1 1 1) plane of $L1_0$ Ni_2FeGa. We note that in order to move atoms at position A to the positon C along $[1\,1\,\bar{2}]$ direction, a high stress is required due to the high energy barrier formed when atoms at A slide over atoms at B in the same plane.

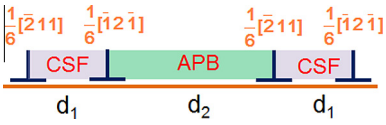

Fig. B1. Separations of partial dislocations for the superdislocation $\frac{1}{2}[\bar{1}\,1\,0]$.

Appendix B. Separations determination of partial dislocations

The separations, d_1 and d_2, of partial dislocations can be calculated using the force balance between attraction due to fault energies and elastic repulsion of partial dislocations (Crawford et al., 1973; Stroh, 1958):

$$\sum F = F_{attraction}(\gamma) - F_{repulsion}(K,d) = 0 \tag{B1}$$

This leads to the following equations for the case of superdislocation $[\bar{1}\,1\,0]$ splitting into four partials $\frac{1}{6}\langle\bar{2}\,1\,1]$ as follows:

$$\gamma_{CSF} = K\left\{\frac{1}{d_1} + \frac{1}{d_1+d_2} + \frac{1}{2d_1+d_2}\right\} \tag{B2}$$

$$\gamma_{APB} - \gamma_{CSF} = K\left\{\frac{1}{d_2} + \frac{1}{d_1+d_2} - \frac{1}{d_1}\right\} \tag{B3}$$

with γ and K/d representing the attraction and elastic repulsion force, respectively. These equations can be solved for the separation distances giving the energy levels and the other material constants as input. As noted earlier, $\gamma_{CSF} = 273$ mJ/m^2 and $\gamma_{APB} = 179$ mJ/m^2. The factor K is given as $K = \frac{\mu b^2}{2\pi}$, where $\mu = 29.5$ GPa (obtained from our simulations), $b = 1.49$ Å. This results in $d_1 = 0.538$ nm and $d_2 = 1.85$ nm shown in Fig. B1.

References

Appel, F., Paul, J.D.H., Oehring, M., 2011. Deformation Behavior of Single-Phase Alloys, Gamma Titanium Aluminide Alloys. Wiley-VCH Verlag GmbH & Co. KGaA, pp. 71–124.
Arndt, M., Griebel, M., Novák, V., Roubíček, T., Šittner, P., 2006. Martensitic transformation in NiMnGa single crystals: numerical simulation and experiments. International Journal of Plasticity 22, 1943–1961.
Barandiarán, J.M., Gutiérrez, J., Lázpita, P., Chernenko, V.A., Seguí, C., Pons, J., Cesari, E., Oikawa, K., Kanomata, T., 2008. Martensitic transformation in Ni–Fe–Ga alloys. Materials Science and Engineering: A 478, 125–129.
Brown, P.J., Crangle, J., Kanomata, T., Matsumoto, M., Neumann, K.U., Ouladdiaf, B., Ziebeck, K.R.A., 2002. The crystal structure and phase transitions of the magnetic shape memory compound Ni_2MnGa. Journal of Physics: Condensed Matter 14, 10159–10171.
Carrez, P., Cordier, P., Mainprice, D., Tommasi, A., 2006. Slip systems and plastic shear anisotropy in Mg_2SiO_4ringwoodite. European Journal of Mineralogy 18, 149–160.
Carrez, P., Ferré, D., Cordier, P., 2007. Peierls–Nabarro model for dislocations in $MgSiO_3$ post-perovskite calculated at 120 GPa from first principles. Philosophical Magazine 87, 3229–3247.
Chumlyakov, Y., Kireeva, I., Panchenko, E., Timofeeva, E., Pobedennaya, Z., Chusov, S., Karaman, I., Maier, H., Cesari, E., Kirillov, V., 2008. High-temperature superelasticity in CoNiGa, CoNiAl, NiFeGa, and TiNi monocrystals. Russian Physics Journal 51, 1016–1036.
Chumlyakov, Y.I., Kireeva, I.V., Panchenko, E.Y., Kirillov, V.A., Timofeeva, E.E., Kretinina, I.V., Danil'son, Y.N., Karaman, I., Maier, H., Cesari, E., 2012. Thermoelastic martensitic transformations in single crystals with disperse particles. Russian Physics Journal 54, 937–950.
Clouet, E., 2012. Screw dislocation in zirconium: an ab initio study. Physical Review B 86, 144104.
Cordier, P., Amodeo, J., Carrez, P., 2012. Modelling the rheology of MgO under Earth's mantle pressure, temperature and strain rates. Nature 481, 177–180.
Coughlin, D., Phillips, P., Bigelow, G., Garg, A., Noebe, R., Mills, M., 2012. Characterization of the microstructure and mechanical properties of a 50.3 Ni-29.7 Ti-20Hf shape memory alloy. Scripta Materialia 67, 112–115.
Crawford, R.C., Ray, I.L.F., Cockayne, D.J.H., 1973. The weak-beam technique applied to superlattice dislocations in iron-aluminium alloys. Philosophical Magazine 27, 1–7.
Dilibal, S., Sehitoglu, H., Hamilton, R., Maier, H., Chumlyakov, Y., 2011. On the volume change in Co–Ni–Al during pseudoelasticity. Materials Science and Engineering: A 528, 2875–2881.
Efstathiou, C., Sehitoglu, H., 2008. Local transformation strain measurements in precipitated NiTi single crystals. Scripta Materialia 59, 1263–1266.
Efstathiou, C., Sehitoglu, H., Carroll, J., Lambros, J., Maier, H.J., 2008. Full-field strain evolution during intermartensitic transformations in single-crystal NiFeGa. Acta Materialia 56, 3791–3799.
Ehmann, J., Fähnle, M., 1998. Generalized stacking-fault energies for TiAl: mechanical instability of the (1 1 1) antiphase boundary. Philosophical Magazine A 77, 701–714.
Ezaz, T., Sehitoglu, H., Maier, H.J., 2011. Energetics of twinning in martensitic NiTi. Acta Materialia 59, 5893–5904.
Ezaz, T., Wang, J., Sehitoglu, H., Maier, H.J., 2013. Plastic deformation of NiTi shape memory alloys. Acta Materialia 61, 67–78.
Fu, C.L., Yoo, M.H., 1992. Deformation behavior of B2 type aluminides: FeAl and NiAl. Acta Metallurgica et Materialia 40, 703–711.
Gall, K., Maier, H., 2002. Cyclic deformation mechanisms in precipitated NiTi shape memory alloys. Acta Materialia 50, 4643–4657.
Hamilton, R.F., Efstathiou, C., Sehitoglu, H., Chumlyakov, Y., 2006a. Thermal and stress-induced martensitic transformations in NiFeGa single crystals under tension and compression. Scripta Materialia 54, 465.
Hamilton, R.F., Sehitoglu, H., Efstathiou, C., Maier, H.J., Chumlyakov, Y., 2006b. Pseudoelasticity in Co–Ni–Al single and polycrystals. Acta Materialia 54, 587.
Hamilton, R.F., Sehitoglu, H., Efstathiou, C., Maier, H.J., 2007. Inter-martensitic transitions in Ni–Fe–Ga single crystals. Acta Materialia 55, 4867–4876.
Hamilton, R.F., Sehitoglu, H., Aslantas, K., Efstathiou, C., Maier, H.J., 2008. Inter-martensite strain evolution in NiMnGa single crystals. Acta Materialia 56, 2231–2236.
Hartford, J., von Sydow, B., Wahnström, G., Lundqvist, B.I., 1998. Peierls barriers and stresses for edge dislocations in Pd and Al calculated from first principles. Physical Review B 58, 2487–2496.
Hartl, D.J., Chatzigeorgiou, G., Lagoudas, D.C., 2010. Three-dimensional modeling and numerical analysis of rate-dependent irrecoverable deformation in shape memory alloys. International Journal of Plasticity 26, 1485–1507.

Please cite this article in press as: Wang, J., et al. Dislocation slip stress prediction in shape memory alloys. Int. J. Plasticity (2013), http://dx.doi.org/10.1016/j.ijplas.2013.08.017

Hosford, W.F., 2005. Mechanical Behavior of Materials. Cambridge University Press.
Joós, B., Duesbery, M.S., 1997. The Peierls stress of dislocations: an analytic formula. Physical Review Letters 78, 266–269.
Joós, B., Ren, Q., Duesbery, M.S., 1994. Peierls–Nabarro model of dislocations in silicon with generalized stacking-fault restoring forces. Physical Review B 50, 5890–5898.
Juan, Y.-M., Kaxiras, E., 1996. Generalized stacking fault energy surfaces and dislocation properties of silicon: a first-principles theoretical study. Philosophical Magazine A 74, 1367–1384.
Karaman, I., Lagoudas, D.C., 2006. Magnetic shape memory alloys with high actuation forces. DTIC Document.
Kibey, S.A., 2007. Mesoscale Models for Stacking Faults, Deformation Twins and Martensitic Transformations: Linking Atomistics to Continuum. ProQuest, pp. 18–20.
Kibey, S., Liu, J.B., Curtis, M.J., Johnson, D.D., Sehitoglu, H., 2006. Effect of nitrogen on generalized stacking fault energy and stacking fault widths in high nitrogen steels. Acta Materialia 54, 2991–3001.
Kokorin, V.V., Martynov, V.V., Chernenko, V.A., 1992. Stress-induced martensitic transformations in Ni2MnGa. Scripta metallurgica et materialia 26, 175–177.
Kresse, G., Furthmuller, J., 1996. Efficient iterative schemes for ab initio total-energy calculations using a plane-wave basis set. Physical Review B (Condensed Matter) 54, 11169.
Kresse, G., Hafner, J., 1993. Ab initio molecular dynamics for open-shell transition metals. Physical Review B (Condensed Matter) 48, 13115.
Lejček, L., 1973. On minimum of energy in the Peierls–Nabarro dislocation model. Czechoslovak Journal of Physics 23, 176–178.
Liu, J., Johnson, D., 2009. Bcc-to-hcp transformation pathways for iron versus hydrostatic pressure: coupled shuffle and shear modes. Physical Review B 79, 134113.
Liu, Y.L., Liu, L.M., Wang, S.Q., Ye, H.Q., 2007. First-principles study of shear deformation in TiAl and Ti3Al. Intermetallics 15, 428–435.
Lu, G., 2005. The Peierls–Nabarro model of dislocations: a venerable theory and its current development. Handbook of Materials Modeling. Springer, pp. 793–811.
Lu, G., Kioussis, N., Bulatov, V.V., Kaxiras, E., 2000. The Peierls–Nabarro model revisited. Philosophical Magazine Letters 80, 675–682.
Martynov, V.V., 1995. X-ray diffraction study of thermally and stress-induced phase transformations in single crystalline Ni–Mn–Ga alloys, C8 ed. Editions de Physique, Lausanne, Switzerland, pp. 91–99.
Masdeu, F., Pons, J., Segui, C., Cesari, E., Dutkiewicz, J., 2005. Some features of Ni–Fe–Ga shape memory alloys under compression. Journal of Magnetism and Magnetic Materials 290–291, 816.
McDowell, D.L., 2010. A perspective on trends in multiscale plasticity. International Journal of Plasticity 26, 1280–1309.
Medvedeva, N.I., Mryasov, O.N., Gornostyrev, Y.N., Novikov, D.L., Freeman, A.J., 1996. First-principles total-energy calculations for planar shear and cleavage decohesion processes in B2-ordered NiAl and FeAl. Physical Review B 54, 13506–13514.
Miranda, C.R., Scandolo, S., 2005. Computational materials science meets geophysics: dislocations and slip planes of MgO. Computer Physics Communications 169, 24–27.
Nabarro, F.R.N., 1947. Dislocation in a simple cubic lattice. Proceedings of the Physical Society 59.
Nabarro, F.R.N., 1997. Theoretical and experimental estimates of the Peierls stress. Philosophical Magazine A 75, 703–711.
Ogata, S., Ju, L., Yip, S., 2005. Energy landscape of deformation twinning in bcc and fcc metals. Physical Review B (Condensed Matter and Materials Physics) 71, 224102.
Oikawa, K., Ota, T., Ohmori, T., Tanaka, Y., Morito, H., Fujita, A., Kainuma, R., Fukamichi, K., Ishida, K., 2002. Magnetic and martensitic phase transitions in ferromagnetic Ni–Ga–Fe shape memory alloys. Applied Physics Letters 81, 5201.
Oikawa, K., Omori, T., Sutou, Y., Kainuma, R., Ishida, K., 2003. Development of the Co-Ni-Al ferromagnetic shape memory alloys. Journal De Physique. IV: JP 112 II, 1017–1020.
Omori, T., Kamiya, N., Sutou, Y., Oikawa, K., Kainuma, R., Ishida, K., 2004. Phase transformations in Ni–Ga–Fe ferromagnetic shape memory alloys. Materials Science and Engineering: A 378, 403–408.
Ozdemir, N., Karaman, I., Mara, N., Chumlyakov, Y., Karaca, H., 2012. Size effects in the superelastic response of $Ni_{54}Fe_{19}Ga_{27}$ shape memory alloy pillars with a two stage martensitic transformation. Acta Materialia 60, 5670–5685.
Paidar, V., 1976. Generalized stacking faults in model lattice of ordered Fe-Si alloys. Czechoslovak Journal of Physics 26, 865–874.
Paidar, V., 2004. Behaviour of dislocations in TiAl intermetallics. Materials Science and Engineering: A 387–389, 977–980.
Peierls, E., 1940. The size of a dislocaiton. Proceedings of the Physical Society 52.
Planes, A., Obrado, E., Gonzalez-Comas, A., Manosa, L., 1997. Premartensitic transition driven by magnetoelastic interaction in BCC ferromagnetic Ni_2MnGa. Physical Review Letters 79, 3926–3929.
Pons, J., Santamarta, R., Chernenko, V.A., Cesari, E., 2005. Long-period martensitic structures of Ni–Mn–Ga alloys studied by high-resolution transmission electron microscopy. Journal of Applied Physics 97.
Romero, R., Lovey, F., Ahlers, M., 1988. Plasticity in β phase Cu–Zn–Al alloys. Philosophical Magazine A 58, 881–903.
Santamarta, R., Font, J., Muntasell, J., Masdeu, F., Pons, J., Cesari, E., Dutkiewicz, J., 2006. Effect of ageing on the martensitic transformation of Ni–Fe–Ga alloys. Scripta Materialia 54, 1105–1109.
Schoeck, G., 1999. Peierls energy of dislocations: a critical assessment. Physical Review Letters 82, 2310–2313.
Segui, C., Chernenko, V.A., Pons, J., Cesari, E., Khovailo, V., Takagi, T., 2005. Low temperature-induced intermartensitic phase transformations in Ni–Mn–Ga single crystal. Acta Materialia 53, 111–120.
Sehitoglu, H., Jun, J., Zhang, X., Karaman, I., Chumlyakov, Y., Maier, H.J., Gall, K., 2001. Shape memory and pseudoelastic behavior of 51.5%Ni–Ti single crystals in solutionized and overaged state. Acta Materialia 49, 3609–3620.
Sehitoglu, H., Wang, J., Maier, H.J., 2012. Transformation and slip behavior of Ni_2FeGa. International Journal of Plasticity 39, 61–74.
Stroh, A.N., 1958. Dislocations and cracks in anisotropic elasticity. Philosophical Magazine 3, 625–646.
Sutou, Y., Kamiya, N., Omori, T., Kainuma, R., Ishida, K., Oikawa, K., 2004. Stress-strain characteristics in Ni–Ga–Fe ferromagnetic shape memory alloys. Applied Physics Letters 84, 1275.
Tadmor, E.B., Miller, R.E., 2011. Modeling Materials: Continuum, Atomistic and Multiscale Techniques. Cambridge University Press.
Timofeeva, E., Panchenko, E.Y., Chumlyakov, Y.I., Maier, H., 2012. Development of thermoelastic martensitic transformations in ferromagnetic [011]-oriented NiFeGa single crystals in compression. Russian Physics Journal, 1–4.
Trinkle, D.R., 2008. Lattice Green function for extended defect calculations: computation and error estimation with long-range forces. Physical Review B 78, 014110.
Ullakko, K., Huang, J.K., Kantner, C., O'Handley, R.C., Kokorin, V.V., 1996. Large magnetic-field-induced strains in Ni_2MnGa single crystals. Applied Physics Letters 69, 1966–1968.
Vitek, V., 1968. Intrinsic stacking faults in body-centred cubic crystals. Philosophical Magazine 18, 773.
Wang, J.N., 1996. Prediction of Peierls stresses for different crystals. Materials Science and Engineering: A 206, 259–269.
Wang, Y., Zheng, Y., Cai, W., Zhao, L., 1999. The tensile behavior of $Ti_{36}Ni_{49}Hf_{15}$ high temperature shape memory alloy. Scripta Materialia 40, 1327–1331.
Wang, G., Strachan, A., Cagin, T., Goddard III, W.A., 2001. Molecular dynamics simulations of 1/2 a ⟨111⟩ screw dislocation in Ta. Materials Science and Engineering: A 309, 133–137.
Whang, S.H., Feng, Q., Gao, Y.Q., 1998. Ordering, deformation and microstructure in L10 type FePt. Acta Materialia 46, 6485–6495.
Wheeler, J.M., Niederberger, C., Tessarek, C., Christiansen, S., Michler, J., 2013. Extraction of plasticity parameters of GaN with high temperature, in situ micro-compression. International Journal of Plasticity 40, 140–151.

Please cite this article in press as: Wang, J., et al. Dislocation slip stress prediction in shape memory alloys. Int. J. Plasticity (2013), http://dx.doi.org/10.1016/j.ijplas.2013.08.017

Whelan, M., Hirsch, P., Horne, R., Bollmann, W., 1957. Dislocations and stacking faults in stainless steel. Proceedings of the Royal Society of London. Series A, Mathematical and Physical Sciences, 524–538.
Wollmershauser, J.A., Kabra, S., Agnew, S.R., 2009. In situ neutron diffraction study of the plastic deformation mechanisms of B2 ordered intermetallic alloys: NiAl, CuZn, and CeAg. Acta Materialia 57, 213–223.
Woodward, C., 2005. First-principles simulations of dislocation cores. Materials Science and Engineering: A 400, 59–67.
Woodward, C., Rao, S., 2002. Flexible ab initio boundary conditions: simulating isolated dislocations in bcc Mo and Ta. Physical Review Letters 88, 216402.
Yu, H.J., Fu, H., Zeng, Z.M., Sun, J.X., Wang, Z.G., Zhou, W.L., Zu, X.T., 2009. Phase transformations and magnetocaloric effect in NiFeGa ferromagnetic shape memory alloy. Journal of Alloys and Compounds 477, 732–735.
Zheludev, A., Shapiro, S.M., Wochner, P., Tanner, L.E., 1996. Precursor effects and premartensitic transformation in Ni_2MnGa. Physical Review B (Condensed Matter) 54, 15045–15050.

Please cite this article in press as: Wang, J., et al. Dislocation slip stress prediction in shape memory alloys. Int. J. Plasticity (2013), http://dx.doi.org/10.1016/j.ijplas.2013.08.017